October 2022

Determining CaMKII Variant Activities and Their Roles in Human Disease

Matthew J. Dunn
University of Massachusetts Amherst

DETERMINING CAMKII VARIANT ACTIVITIES AND THEIR ROLES IN HUMAN DISEASE

A Master's Thesis Presented

by

Matthew Dunn

Submitted to the Graduate School of the
University of Massachusetts Amherst in partial fulfillment
of the requirements for the degree of

MASTER OF SCIENCE

September 2022

Molecular and Cellular Biology

DETERMINING CAMKII VARIANT ACTIVITIES AND THEIR ROLES IN HUMAN DISEASE

A Master's Thesis Presented

by

Matthew Dunn

Approved as to style and content by:

_____

Chair, Dr. Margaret M. Stratton

_____

Member, Dr. Peter Chien

_____

Member, Dr. Rafael A. Fissore

_____

Dr. Tom Maresca

Graduate Program Director

Molecular and Cellular Biology

ACKNOWLEDGEMENTS

This work was supported by a grant from the National Institute of General Medical Sciences. I especially want to thank Dr. Margaret Stratton and all other members of the Stratton Lab their mentorship and friendship throughout my time in the Stratton Lab. Thank you to my friends and family for all your support over the years and continued support as I continue my graduate education.

ABSTRACT

DETERMINING CAMKII VARIANT ACTIVITIES AND THEIR ROLES IN HUMAN DISEASE

SEPTEMBER 2022
MATTHEW DUNN, B.S., UNIVERISTY OF MASSACHUSETTS AMHERST
M.S., UNIVERSITY OF MASSACHUSETTS AMHERST
Directed by: Professor Margaret M. Stratton

Ca^{2+}/calmodulin-dependent protein kinase II (CaMKII) is involved in Ca^{2+} signaling throughout the body. CaMKII is enriched in the hippocampus and required for learning and memory formation. Four highly conserved genes encode CaMKII in vertebrates: α, β, γ, and δ. All CaMKII variants are constituted of a kinase domain, regulatory segment, variable linker, and hub domain. These domains comprise an individual subunit which oligomerize together via the hub domain to form multimeric holoenzymes. These four genes are most variable in the linker domain due to extensive alternative splicing. The variable linker significantly impacts the activation of CaMKIIα. Herein, I attempt to develop an *in vitro* assay which resembles physiological activation of CaMKII via Ca^{2+} oscillations. I provide preliminary data which indicate that alternative splicing of the variable linker in CaMKIIα modulates the Ca^{2+} frequency dependent autonomy of these variants. Additionally, neuronal CaMKII variants of CaMKIIα and CaMKIIβ decode Ca^{2+} oscillations into different levels of autonomous activity. Lastly, I assess the impacts of three *de novo* mutations (Q274P, R275H, and F294S) on Ca^{2+}/CaM sensitivity in CaMKIIδ by providing data that these 3 mutants increase the sensitivity of CaMKIIδ to Ca^{2+}/CaM and that Q274P and F294S mutants display Ca^{2+}/CaM independent activity.

TABLE OF CONTENTS

LIST OF FIGURES

LIST OF ABBREVIATIONS

Ca^{2+}/calmodulin-dependent protein kinase II (CaMKII); long-term potentiation (LTP); long-term depression (LTD); calmodulin (CaM); calcium (Ca^{2+}); calcium-bound calmodulin (Ca^{2+}/CaM); post-translation modifications (PTMs); α-amino-3-hydroxy-5-methyl-4-isoxazolepropionic acid (AMPA); N-methyl-D-aspartate (NMDA); small-angle x-ray scattering (SAXS); matrix-assisted laser desorption/ionization time-of-flight mass spectrometry (MALDI-TOF MS)

CHAPTER 1

INTRODUCTION

Memory enables the ability to store information and experiences in the brain for short-term and long-term use. Our memories are integral to our self-perception, relationships, decisions, and our overall awareness of our environment. However, the molecular basis of memory formation and information storage has not been entirely elucidated. Specifically, memories are maintained for long periods of time, whereas proteins and other biomolecules turnover within minutes, days, or weeks.

In 1984, Francis Crick proposed criteria for a "memory molecule" to address this conundrum. Crick argued the molecule must be an oligomeric enzyme that was able to transfer activation between subunits; also, post-translation modifications (PTM), such as phosphorylation or methylation, must modulate the activation state of the enzyme (Crick, 1984). Together, these mechanisms could allow for perpetuation of a molecular signal well past protein turnover and explain the molecular mechanism of memory. The following year John Lisman proposed a mechanism for the storage of information via a kinase capable of auto-phosphorylation (Lisman, 1985). Like Crick's, this model required propagation of a PTM between molecules. An external stimulus would activate the primary kinase, whose activity state is controlled by a phosphatase. Once activated, the primary kinase could phosphorylate additional kinases within a different holoenzyme *in trans*. Lisman proposed this must occur in the absence of the original stimulus leading to a mechanism for memory storage insensitive to molecular turnover.

Meanwhile, a calmodulin-dependent protein kinase was discovered at high concentration in postsynaptic densities and demonstrated the ability to autophosphorylate (Kennedy et al., 1983a). This same protein kinase corresponded to previously identified targets of calcium-calmodulin (Ca^{2+}/CaM) dependent phosphorylation from various tissues (Schulman & Greengard, 1978a, 1978b). Together, these results supported that autophosphorylation is a physiologically relevant mechanism (Bennett et al., 1983; Kennedy et al., 1983b). This protein kinase would later become known as Ca2+/calmodulin-dependent protein kinase II (CaMKII). CaMKII is now known to be essential to long-term potentiation (LTP) which is the model underlying the cellular basis of memory and information storage via synaptic plasticity (Herring and Nicoll, 2016).

Long-term potentiation

Learning and memory are adaptable processes which change with experiences. Synapses, which are connections between neurons, could contribute to the maintenance of these processes. Later, the discovery of long-term potentiation supported these models; stimulation of hippocampal excitatory neurons resulting in a rapid and lasting increase in the strength of the synapses (Bliss and Lømo, 1973). LTP induction requires the activation of postsynaptic N-methyl-D-aspartate (NMDA) receptors (Collingridge et al., 1983) leading to calcium (Ca^{2+})influx into the postsynaptic neuron. Upon entry through NMDA and α-amino-3-hydroxy-5-methyl-4-isoxazolepropionic acid (AMPA) receptors (Bashir et al., 1991; Wollmuth and Sakmann, 1998), Ca^{2+} binds to calmodulin (CaM) which induces an extensive conformational change (Zhang et al., 1995). Ca^{2+}/CaM competitively binds to the CaM footprint of the regulatory segment which displaces the regulatory segment from the substrate recognition site, enabling kinase activity (Lin and Redmond, 2009). Active CaMKII is able to phosphorylate AMPA receptors which

translocate to the postsynaptic density (PSD) (Shi et al., 1999) and leads to a rapid increase AMPA receptors at the synapse (Patterson et al., 2010). More recently transient inhibition of CaMKII at excitatory synapses caused long-term deficits in LTP implicating CaMKII as a storage device (Tao et al., 2021).

Additionally, CaMKII is involved with the structural reorganization of dendritic spines during LTP. Specifically, CaMKIIβ bundles F-actin, which composes the primary skeleton in the dendritic spin (Okamoto et al., 2007). This interaction is independent of kinase activity, and upon kinase activation CaMKII detaches from F-actin which allows for reorganization of other signaling machinery. Upon deactivation of CaMKII, it is then able to rebind F-actin and stabilize the newly remodeled spine structure (Okamoto et al., 2007). Thus, CaMKII plays an essential role in the underlying structural mechanisms that strengthen synapses. Taken together this work solidifies CaMKII as both necessary and sufficient for the induction of LTP (Lisman et al., 2002; Herring and Nicoll, 2016).

CaMKII activation

CaMKII biochemistry and structure must be well characterized for comprehensive understanding of the mechanisms of learning and memory. CaMKII is a serine/threonine oligomeric kinase which assembles into holoenzymes of 12-14 subunits. Each subunit consists of a kinase domain, regulatory segment, variable linker domain, and hub domain (Stratton et al., 2014). CaMKII is a particularly unique kinase due to the mode of autoinhibition and high order oligomeric conformations. In its autoinhibited conformation, the regulatory segment occludes the substrate

binding site of the kinase domain, preventing substrate binding. Upon Ca^{2+}/CaM binding the regulatory segment, the kinase domain undergoes a conformational change, exposing the substrate binding site. The kinase domain is then able to phosphorylate additional subunits *in trans* at Threonine 286 leading to CaMKII activation. Thr286 is located within the regulatory segment and phosphorylation prevents the regulatory segment from binding to the kinase domain, resulting in constitutive CaMKII activity (Giese et al., 1998). Following T286 phosphorylation, CaMKII is persistently active in the absence of Ca^{2+}/CaM and can continuously auto-phosphorylate additional adjacent subunits at Thr286 and Thr305/306. Thr305/306 are considered inhibitory phosphorylation sites because phosphorylation of these residues prevents binding of Ca^{2+}/CaM (Patton et al., 1990). CaMKII phosphorylation is specifically crucial to LTP. Severe memory and spatial learning deficits were observed in transgenic mice with mutations at Thr286, and rigid learning was observed in mice with mutated Thr305/306 (Giese et al., 1998). More generally, mice deficient in neuronal CaMKIIα and CaMKIIβ display learning impairments and have limited long-term memory (Borgesius et al., 2011; Silva et al., 1992) suggesting a crucial role for CaMKII in memory and learning.

CaMKII expression and alternative splicing

In conjunction with activation of CaMKII its expression is equally complex. There are four CaMKII paralogs in humans, α, β, γ, and δ, which generate more than 70 CaMKII splice variants in the hippocampus via variable splicing primarily in the linker domain (Sloutsky et al., 2020). Across the four human CaMKII paralogs, there is high conservation of the kinase and hub domains, 90 and 75% minimum pairwise identity, respectively (Sloutsky et al., 2020). On the contrary, the linker connecting the kinase and regulatory segment to the hub is highly variable in

composition and length due to variable splicing, although some exons are highly conserved between genes (Sloutsky and Stratton, 2020; Sloutsky et al., 2020). The α and β paralogs are expressed predominantly in neurons, whereas γ and δ are widely distributed throughout the body (Tombes et al., 2003).

Previous structural analysis of full-length CaMKII was achieved by Chao et al. (2011); they solved a crystal structure of autoinhibited full-length CaMKIIα. The construct contained no variable linker region and revealed a compact form where the kinase domains were docked against the hub domain. The crystal structure also revealed that the CaM binding sites located within the regulatory segment were inaccessible in this conformation. To further understand how the linker contributes to CaMKII structure, the researchers conducted small angle x-ray scattering (SAXS) reconstructions on several constructs; specifically, they compared a short linker (0 aa residue linker) and long linker (30 aa residue linker) construct. In comparison, the longer linker SAXS reconstruction revealed an extended conformation in which the kinases were not directly contacting the hub domain. To further solidify their data, they carried out biochemical assays to determine the EC_{50} of each construct. These experiments revealed a higher sensitivity to Ca^{2+}/CaM for the longer linker variant (12 nM) than the short linker variant (6 μM). From this data they proposed a dynamic equilibrium between the more compact form and the extended position of the kinase domains, with respect to the hub domains, which is tuned by the linker length. Thus, variants with a longer linker will be observed in the extended form more often and will be more easily activated due to the easier access to the CaM binding sites.

These data revealed an important role for the linker domain in CaMKII activation and activity, but it was limited to a small number of possible variants. Sloutsky et al. (2020) sought to test this hypothesis on a larger number of variants. They utilized deep sequencing of human hippocampal samples to detect more than 70 CaMKII transcripts from all four paralogs. Next, they implemented the same assay as Chao et al. (2011) to characterize the Ca^{2+}/CaM sensitivity of CaMKIIα and CaMKIIβ variants with a range of linker composition and lengths. Their assays revealed that CaMKIIα sensitivity to Ca^{2+}/CaM was tuned by linker length, with longer variants being more easily activated or having a lower EC_{50} than shorter variants (consistent with Chao et al. 2011). On the contrary, the CaMKIIβ variants they tested displayed no significant variation in their sensitivity to Ca^{2+}/CaM despite variation in linker lengths (0 to 217 aa). Interestingly, the CaMKIIβ variant with a 0 aa linker had an EC_{50} of 21 nM which is similar to the EC_{50} of CaMKIIα with a 30 aa linker (24 nM) but significantly lower than that of CaMKIIα with a 0 aa linker (313 nM). Thus, other domains must be contributing to Ca^{2+}/CaM sensitivity. Researchers designed chimera constructs of CaMKIIα and CaMKIIβ consisting of α kinase/β hub and β kinase/α hub. These chimeras were subjected to the same assay and their results reveal an allosteric role for the hub domain in CaMKII activity (Sloutsky et al., 2020).

CaMKII transduces Ca^{2+} oscillations

The measurements used by Chao et al. (2011) and Sloutsky et al. (2020) to characterize sensitivity to Ca^{2+}/CaM were recorded at equilibrium Ca^{2+} conditions, but it is known that CaMKII activity is dependent on the frequency of Ca^{2+} oscillations in postsynaptic neurons (De Koninck & Schulman, 1998; Bayer et al., 2002; Chao et al., 2011). These bursts of Ca^{2+} influx are due to action potential propagation and timed frequency of these oscillation are believed to

encode crucial information to LTP (Brown et al., 2000; De Koninck and Schulman, 1998). Additionally, Ca^{2+} is used throughout the human body as a cellular signal, specifically fluctuations intracellular concentrations encode a variety of signals. In neurons, stimulus frequency-dependent changes in Ca^{2+} synapse transmission, such as LTP, involve CaMKII suggesting a role in decoding these synaptic inputs (De Koninck & Schulman, 1998).

To understand this role, De Koninck and Schulman immobilized CaMKII via an HA tag/antibody. They used pressurized perfusion chambers to pulse the immobilized CaMKII with Ca^{2+}, CaM, and ATP followed by EGTA. Autophosphorylation at Thr^{286} requires binding of CaM to subunits *in trans.* As a result, submaximal activation of CaMKII by a single Ca^{2+} spike may fail to result in autophosphorylation, but repeated spikes may lead to accumulation of autonomous activity. Therefore, they measured phosphorylation at Thr^{286} following pulsing as an indication of autonomy. Their results indicated that higher frequencies resulted in higher levels of autonomy (Thr^{286} phosphorylation) (De Koninck & Schulman, 1998). Bayer et al. conducted a similar experiment, with three CaMKIIβ variants. Their results also indicated an increase in autonomous levels with the frequency of Ca^{2+} oscillations. Differences in the kinase position, relative to the hub domain, due to the variable linker allows for nuanced differences in activation and variable expression in hippocampal neurons provide a mechanism to modulate neuron sensitivity to Ca^{2+} oscillations (Bayer et al., 2002). Lastly, Chao et al. demonstrated variable responses to Ca^{2+} oscillations between different CaMKIIα variants. Using a similar experimental setup, they exposed CaMKIIα 0 aa linker and CaMKIIα 30 aa linker to Ca^{2+} oscillations. They observed similar patterns between autonomy and frequency of Ca^{2+} oscillations and

demonstrated that CaMKIIα 0 aa linker required higher frequencies to reach the same percent autonomy as CaMKIIα 30 aa linker (Chao et al., 2011).

The role of CaMKII in human disease

Historically CaMKIIα and CaMKIIβ have been the focus of many neurological studies, as they represent 2% of the total hippocampal protein (Erondu and Kennedy, 1985). However, more recently, CaMKIIγ and CaMKIIδ missense mutations have been associated with numerous neurological disabilities indicating an essential role for all CaMKII paralogs in neurological development and function (Küry et al., 2017; Onori et al., 2018). Aberrant synaptic plasticity is an underlying mechanism which causes multiple neurological and psychiatric disorders (Bliss et al., 2014). Specifically, dysfunctional ionotropic glutamate receptors, α-amino-3-hydroxy-5-methyl-4-isoxazole propionic acid receptors (AMPAR) and N-methyl-D-aspartate receptor (NMDAR), are the cause of many neurological disorders (Barkus et al., 2014; Lau and Zukin, 2007; Zhang and Abdullah, 2013). CaMKII had not been associated with neurological disorders historically. However, with the advent of new sequencing technologies many missense mutations in all four genes have been found to impact CaMKII activity, autonomy, and localization within neurons, suggesting a causative role for a range of neurological disorders (Chia et al., 2018; Küry et al., 2017; Robison, 2014; Stephenson et al., 2017). In some cases, causative links have been established (Küry et al., 2017; Onori et al., 2018; Stephenson et al., 2017), but it is not understood how mutant CaMKII alleles exert dominance over wild-type CaMKII alleles causing neuronal dysfunction in heterozygous individuals.

This thesis aims to further characterize two biochemical properties of CaMKII which are crucial to our understanding of its role in learning and memory. First, how does alternative splicing within the variable linker region impact the ability of CaMKII to decode Ca^{2+} oscillations? Previous work demonstrates that the linker length tunes the levels of autonomous activity in response to these Ca^{2+} oscillations. I hope to extend this model to a wider range of hippocampal CaMKII variants and develop a method to measure in vitro CaMKII activation under more relevant conditions. Second, I hope to extend research focused on de novo CaMKII mutations.

CHAPTER II

HIPPOCAMPAL CaMKII VARIANTS DIFFERETIALLY DECODE CA^{2+} OSCILLATIONS

Matthew J. Dunn[1], Margaret M. Stratton[2]
Department of Molecular and Cellular Biology[1]
Department of Biochemistry and Molecular Biology[2]

Abstract

Calcium/calmodulin-dependent protein kinase II (CaMKII) plays an integral role in Ca^{2+} signaling throughout the body. CaMKII is required for long term potentiation (LTP), the molecular mechanism which underlies memory and learning. In vertebrates there are four CaMKII paralogs: CaMKIIα, CaMKIIβ, CaMKIIγ, and CaMKIIδ. Each gene encodes a kinase domain, a regulatory segment, a variable linker, and a hub domain. All four CaMKII genes are highly conserved, and the variable linker region has conserved exon boundaries which undergo extensive alternative splicing. These splice variants have been shown to change CaMKII sensitivity to Ca^{2+} which is responsible for CaMKII activation *in vivo.* CaMKII activation and autonomy through T286 phosphorylation lead to long-lived changes in dendritic spine structure and gene expression. I show that in vitro CaMKIIα splice variants demonstrate variable levels of Ca^{2+} frequency-dependent autonomous activity depending on the length of the variable linker region, and CaMKIIα and CaMKIIβ decode these oscillations into different levels of autonomy. Therefore, variable splicing modulates the autonomous activity of CaMKII *in vitro*, which has meaningful implications about the specificity of CaMKII activation by Ca^{2+} oscillations and may further explain its essential role in synaptic plasticity and LTP.

Introduction

Calcium (Ca^{2+}) is a ubiquitous secondary messenger and Ca^{2+} signaling is pervasive throughout cellular signal transduction pathways (Catterall, 2011). In neurons, changes in intracellular Ca^{2+} concentration occur as spikes or oscillations which transmit the depolarization signal and impact synaptic activity. Additional information may be communicated by the amplitude, frequency, and duration of Ca^{2+} oscillations (De Koninck and Schulman, 1998). Ca^{2+} frequency-stimulated changes in synaptic activity, such as long-term potentiation (LTP) and long-term depression (LTD), require activation of Ca^{2+}/calmodulin-dependent protein kinase II (CaMKII) (Lisman et al., 2012). CaMKII activity is particularly unique because it can decode cellular information transduced by Ca^{2+} oscillations which may be crucial to its role in LTP induction at the synapse (De Koninck and Schulman, 1998; Chao et al., 2011; Bayer et al., 2002).

Historically, EC_{50} has been used as a metric to quantify differences in the concentration of Ca^{2+}/CaM required for activation of CaMKII splice variants (Chao et al., 2011; Sloutsky et al., 2020). A CaMKIIα variant with a 30-residue linker requires significantly less Ca^{2+}/CaM to achieve maximal activity than a CaMKIIα variant with a 0-residue linker (Chao et al., 2011; Sloutsky et al., 2020). On the other hand, a CaMKIIβ variant with a 217-residue linker requires approximately the same Ca^{2+}/CaM to reach maximal activity as a CaMKIIβ variant without a linker (Sloutsky et al., 2020), yet CaMKIIβ variants have demonstrated differential levels of autonomy due to Ca^{2+} oscillations (Bayer et al., 2002). The difference in these activation properties reveal an important distinction between CaMKII activation due to Ca^{2+} oscillations compared with steady-state Ca^{2+} conditions. However, intracellular Ca^{2+} concentrations fluctuate with calcium channel activity (Catterall, 2011). Ca^{2+} influx is mainly dependent upon membrane

potential and presynaptic neurotransmitter release, whereas homeostasis of intracellular Ca^{2+} concentrations are controlled by the mitochondria and endoplasmic reticulum (Gleichmann and Mattson, 2011). Thus, activation properties of CaMKII variants may be better understood by stimulating these Ca^{2+} oscillations *in vitro*. Although previous experiments (Bayer et al., 2002; Chao et al., 2011) have assessed the differential activation of some CaMKII splice variants due to Ca^{2+} oscillations, by conducting similar experiments to these with the full array of CaMKIIα and CaMKIIβ splice variants detected using RNA-seq (Sloutsky et al., 2020) we will be able to develop a more accurate model of how the linker affects physiological meaningful CaMKII activation. Specifically, in these experiments we measure the levels of autonomous CaMKII autonomous activity following exposure to various Ca^{2+} oscillations. Significant differences between splice variants in autonomous activity following Ca^{2+} oscillations could allow for specific tuning of synaptic plasticity and CaMKII activity crucial to LTP.

Methods and Materials

Plasmid Construction

A gene fragment (IDT) containing AviTag (Beckett et al., 1999) followed by a C-terminal flexible linker (aa: GASAGSAGS) were subcloned into preexisting pET CaMKII vectors containing N-terminal 6xHIS followed by a SUMO tag (Sloutsky et al., 2020). The AviTag insert was positioned immediately after a Ulp1 cleavage site and positioned at the N-terminus of each CaMKII gene. These vectors were assembled using Gibson assembly and confirmed via Sanger Sequencing (GeneWiz).

CaMKII Expression and Purification

A previously established bacterial expression system (Choa et al., 2010) for CaMKII by coexpression with Lambda Phosphatase was utilized. We expressed CaMKII in *Escherichia coli* by coexpressing with λ phosphatase (from Kuriyan Lab) in Rosetta (DE3)pLysS competent cells (Novagen). λ phosphatase was expressed via a pCDFDuet1 vector and N-terminally clones 6xHis AviTag CaMKII was expressed in a pET287 vector. Cells were grown to an O.D. (595 nm) of 0.6 and induced with 1 mM isopropyl β-D-1-thiogalactopyranoside (IPTG; GoldBio). Cells were grown for 16 hours at 18 °C and resuspended in buffer A [25 mM tris-HCl (pH 8.5), 150 mM KCl, 50 mM imidazole, 10% glycerol; Sigma] with 25 mM magnesium chloride, containing a cocktail of protease inhibitors and deoxyribonuclease (DNase) [0.2 mM 4 benzenesulfonyl fluoride hydrochloride (AEBSF), 5.0 μM leupeptin, pepstatin (1 μg/ml), aprotinin (1 μg/ml), trypsin inhibitor (0.1 mg/ml), 0.5 mM benzamidine, DNase (1 μg/ml)] (Sigma). Resuspended cells were flash frozen until used.

Cells were lysed via a French press and clarified cell lysate was aspirated from cell debris following centrifugation (18,000 rpm; 4 °C; 60 min). All subsequent purification steps were performed with an ÄKTA pure chromatography system (Cytiva Life Sciences) at 4 °C. Clarified cell lysate was loaded onto 2 5-mL HisTrap FF NiNTA Sepharose columns (Cytiva Life Sciences) and eluted with a combination of 50% buffer A and 50% buffer B [25 mM tris-HCl (pH 8.5), 150 mM KCl, 1 M imidazole, 10% glycerol] for a final concentration of 0.5 M imidazole. The eluate was desalted of residual imidazole with a HiPrep 26/10 Desalting column, and His SUMO tags were cleaved with Ulp1 protease overnight at 4°C in buffer C [25 mM tris-HCl (pH 8.5), 150 mM KCl, 2 mM tris(2-carboxyethyl)phosphine (TCEP) (GoldBio), 50 mM imidazole, 10% glycerol]. Cleaved tags were removed by a subtractive NiNTA step.

Subsequently, and anion exchange step was performed with 2 5-mL HiTrap Q-FF (Cytiva Life Sciences) and protein was eluted with a KCl gradient. Eluted proteins were visualized via SDS-PAGE and select fractions were concentration and further purified in gel filtration buffer [25 mM tris-HCl (pH 8.0), 150 mM KCl, 1 mM TCEP, 10% glycerol] using a Superose 6 Increase 10/300 size exclusion column (Cytiva Life Sciences). Fractions were visualized by SDS-PAGE, and pure fractions were pooled, concentrated, aliquoted, flash-frozen in liquid nitrogen, and stored at -80 °C until used. Protein concentration was calculated using absorbance (280 nm).

Calmodulin Purification

Calmodulin (*Gallus gallus*) was recombinantly expressed from a pET-15b vector (a gift from A. Nairn, Yale School of Medicine) in BL21(DE3) cells (Millipore). Cells were grown to an O.D. (595 nm) of 0.6 and induced with 1 mM isopropyl β-D-1-thiogalactopyranoside (IPTG; GoldBio). Cells were grown for 16 hours at 18 °C and resuspended in cell lysis buffer [40 mM tris-HCl (pH 8.0), 100 mM KCl, 10 mM EDTA]. Resuspended cells were flash frozen until used. Cells were lysed via a French press and clarified cell lysate was aspirated from cell debris following centrifugation (18,000 rpm; 4 °C; 60 min). All subsequent purification steps were performed with an ÄKTA pure chromatography system (Cytiva Life Sciences) at 4 °C. Clarified cell lysate was loaded onto 2 5-mL HiTrap Phenyl FF (Low Sub) columns (Cytiva Life Sciences). Column flow through was collected and $CaCl_2$ was added to the flow through (final concentration 20 mM $CaCl_2$). The flow through was applied to a different pair of 5-mL HiTrap Phenyl FF (Low Sub) columns (Cytiva Life Sciences) with buffer A [50 mM tris-HCl (pH 7.5), 1mM $CaCl_2$]. The column was washed sequentially with buffer A, buffer B [50 mM tris-HCl (pH 7.5), 500 mM NaCl, 1 mM $CaCl_2$], and buffer A. Calmodulin was eluted with buffer C [50 mM

tris-HCl (pH 7.5), 2 mM EDTA]. Purity was assessed via SDS-PAGE and clean eluate fractions were pooled and concentrated. To quantify calmodulin concentration, we used circular dichroism on a Jasco J-1500 spectrophotometer to make a measurement in triplicate for our purified sample scanning a wavelength spectrum between 250 and 215 nm to measure the characteristic wavelength of 222 nm as previously described (Harmat et al., 2000). We calculated the calmodulin concentration as follows:

$$[calmodulin](nM) = \frac{1000 \times (CD_{sample}^{222\ nm} - CD_{blank}^{222\ nm})}{\Theta \times l \times number\ of\ amino\ acids}$$

where the circular dichroism at 222 nm (CD222nm) is expressed in mdeg, Θ is the molar ellipticity, and l is the path length in cm.

Frequency Experiment

Dyanbeads MyOne Sptetavidin C1 (ThermoFisher Scientific) are used to bind purified CaMKII. Beads are suspended with 10X volume of frequency buffer [25 mM tris-HCl (pH 7.5), 150 mM KCl] and concentrated with magnet. Supernatant is removed and the wash is repeated 3 times. CaMKII (2.5 μM final concentration) is incubated with beads in frequency buffer and 1 mM TCEP (GoldBio) for 90 minutes at 4 °C while rotating at 25 rpm in a microcentrifuge tube. Following incubation, the beads are concentrated and the wash is repeated 3 times. Protein-bound beads are resuspended in 10.1X volume of frequency buffer.

For control of the pulsing, an automate perfusion system is used; the pulses are controlled by a Valve Bank II (Automate Scientific). Each program consists of 60 activating pulses, each one is

100 ms long with activation buffer [25 mM tris-HCl (pH 7.5), 150 mM KCl, 8 μM CaM, 500 μM $CaCl_2$, 10 mM $MgCl_2$, 250 μM ATP] for a total exposure of 6 s. Each activating pulse is followed immediately by a 50 ms EGTA pulse with chelating buffer [25 mM tris-HCl (pH 8.0), 1.2 mM EGTA] for a total exposure of 3 s. The frequency of the activating and EGTA pulse determine the frequency. Following all 60 pulses, the program ends with a 400 ms pulse of chelating buffer. All buffers are maintained at room temperature (24.8-26.7 ℃) and the pressure of the perfusion system is maintained at 6 PSI for all pulses. Prior to the beginning of each experiment, the output tubing was secured to a magnet with tape. The tubing was filled with frequency buffer. Next 100 μL of protein-bound beads were loaded into the tubing and washed with 400 μL of frequency buffer. The program was run and following completion of each program 3, 300 ms pulses of frequency buffer were used to wash the beads (see Fig. 1 for set up). The tubing was removed from the magnet and flicked to mechanically detach the protein-bounds beads from the tubing. Another 300 ms pulse of frequency buffer was used to remove the protein from the tubing into a microcentrifuge tube. The beads were concentrated with the magnet and resuspended in 35 μL of frequency buffer.

Activity was measured with the ADP Hunter Plus Assay (DiscoveRx). Each well of the plate contained master mix composed of the following (all concentrations listed as final, working concentrations): 75 mM tris-HCl (pH 7.5), 15 mM $MgCl_2$, 100 μM ATP, 300 μM Syntide. For each pulse experiment, 6 reactions were run; 2 of these reactions contained 10 μM CaM and 4 of these reactions contained no calmodulin (25 mM tris-HCl (pH 7.5) was used instead. In addition, each time a frequency experiment was conducted, 3 reactions of reagents only were run as a minimum fluorescent value. The order of addition to each well was 4 μL master mix, 1 μL

CaM/Tris, and the reaction was initiated with 5 µL of protein-bound beads. Following 5 minutes at room temperature 2 µL of stop solution [8.3 mM EDTA, 0.3 mM EGTA] was added to the reaction. Next, 5 µL of Solution A (DiscoveRx) and 10 µL of Solution B (DiscoveRx) were added to each well immediately after the other. The reactions incubated for 15 minutes at room temperature. The fluorescence (590 nm) was measured with a Synergy H1 microplate reader (BioTek). For each pulse experiment, the percent autonomy was calculated using the equation below:

$$Percent\ Autonomy = \frac{\overline{RFU_{frequency}} - \overline{RFU_{min}}}{\overline{RFU_{max}} - \overline{RFU_{min}}}$$

The average fluorescence of the reagent only reactions (RFU_{min}) was subtracted from both the average fluorescence of the +CaM reactions (RFU_{max}) and the tris reactions ($RFU_{frequency}$). Autonomy was calculated by dividing the adjusted average of $RFU_{frequency}$ by that of RFU_{max}. This allowed for normalization of protein concentration within each pulse experiment.

Mass Spectrometry

Biotinylation of N-terminal AviTag CaMKII occurred during bacterial expression and was confirmed with MALDI-TOF MS (IALS MS Core Facility).

SDS-PAGE Densitometry Analysis

Protein samples of unknown concentration were diluted 1:10 and 1:5. 8 µL of each sample were loaded onto a 12% bis-acrylamide (GoldBio) SDS-gel. A standard (CaMKIIα 0 aa linker with a N-terminal AviTag) of known concentration (50.4 µM) underwent the same dilutions. The gel was run at 230 mV for 40 minutes. The gel was stained with Coomassie Blue (GoldBio) and

imaged using. The image was processed with imageJ. Each band corresponding to CaMKII was quantified and normalized to the intensity of the standard. The normalized value was multiplied by the rates gathered from correlating kinase assays to account for differences in protein concentration.

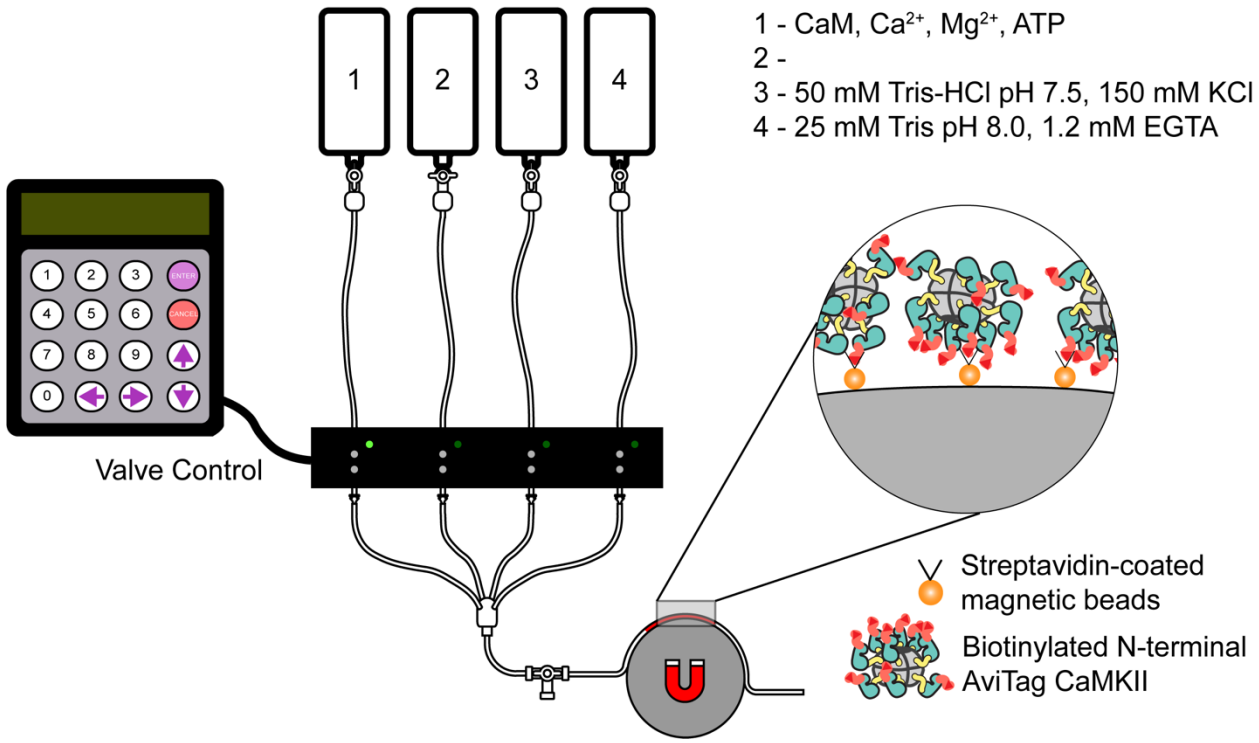

Figure 1. Perfusion System experimental set up. The CaMKII bound beads are injected into tubing secured to the magnet with tape. Meanwhile the system is pressurized to 6 PSI and the channels are filled with buffer according to the labels. Pulsing is controlled by the valve bank controller. All programs contain 6s of total exposure to Ca^{2+}/CaM; the number of EGTA pulses is equal to the number of Ca^{2+}/CaM pulses and remains 50 ms through all the programs. Frequency programs contain 100 ms Ca^{2+}/CaM pulses and range from 0.5 to 6 Hz (120 to 10s, respectively). Pulse duration programs are all at 1 Hz and contain Ca^{2+}/CaM pulses ranging from 50 ms to 200 ms (120 pulses to 30 pulses, respectively). Following pulse experiment and 400 ms EGTA pulse, beads are removed from tubing by 300 ms pulse with Tris KCl.

Results

The transduction of Ca^{2+} signaling by CaMKII is dependent on the amplitude, frequency, and duration of Ca^{2+} oscillations which are decoded into specific levels of CaMKII autonomy via phosphorylation of T286 (De Koninck and Schulman, 1998). Previous work extended this model

to some CaMKIIα (Chao et al., 2011) and CaMKIIβ splice variants (Bayer et al., 2002). In both cases, it was observed that the alternative linker tuned CaMKII autonomy in response to Ca^{2+} oscillations. I attempted to extend this work to fully characterize hippocampal CaMKII variants, but first it was crucial to establish and develop the procedure for these measurements. A system like that described by Chao et al. (2011) was used as a starting point. The largest immediate difference being the relocation of a C-terminal biotynlation sequence (AviTag) to the N-terminus. The tag was moved away from the hub domain at the C-terminus to reduce any impact on oligomerization. The addition of the tag at the N-terminus initially appeared to decrease the

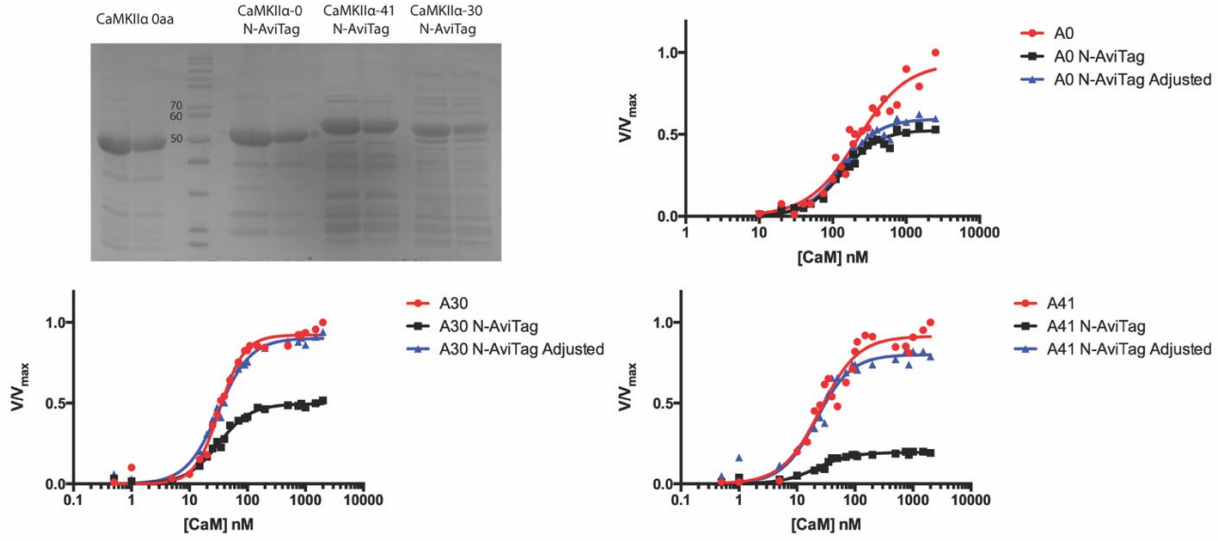

Figure 2. Addition of N-terminal AviTag does not impact CaMKIIα sensitivity to Ca2+/CaM. 12% SDS-PAGE gel of purified CaMKII N-AviTag constructs stained with Coomassie Brilliant Blue. AviTag constructs had high DNA contamination, so CaMKIIα-0 was used as a loading control. Densitometry was analyzed using imageJ and the approxiamate concentrations were normalized to that of CaMKIIα-0. Kinase Assays were completed as described above. Plotted in red is the variant without a tag. Plotted in black is the raw data for the variants containing N-terminal AviTags. Plotted in blue is the kinase assay data adjusted using the determined concentrations from densitomery analysis of the SDS-PAGE.

activity of CaMKIIα hippocampal variants (Fig. 2). However, when the samples were analyzed via SDS-PAGE it was determined there were variable protein concentrations and when kinetic rates were normalized to protein concentrations the addition of the N-terminal AviTag did not affect CaMKII activation (Fig. 2, Fig. S1, Fig. S2, Fig. S3).

Next, I assessed the ADP Hunter Plus Assay (DiscoveRx) for measuring CaMKII autonomy. To ensure that any change in fluorescence was a result of only CaMKII activity several controls were performed which ruled out fluorescence changes from the addition of other reagents such as the magnetic beads or CaM (Fig. 3A). Taken together these data demonstrated that CaM and beads did not impact the efficacy of the assay to detect changes in ADP concentration through fluorescence. Additionally, an ADP titration (Fig. S4) and CaMKII titration (Fig. S5) confirmed a linear relationship between both conditions and fluorescence. Further, I performed a continuous reading of the fluorescent values produced by the ADP Hunter reactions over the course of 1 hour (maximum incubation recommended by DiscoveRx) and found no significant change in the fluorescence of autonomous activity following 15 minutes of incubation.

Following systematic dissection of the fluorescent assay I turned my attention towards the perfusion system. The CaM and EGTA concentrations, 8 μM and 1 mM respectively, were taken from the experimental design described by Chao et al. (2011). In addition, a four-way connection was used to combine the different solutions of the perfusion system (Fig. 1). Lastly, the perfusion system was pressurized to 6 PSI (personal communication with Dr. Meg Stratton) as previously used I began conducting pulse experiments but was unable to obtain consistent results from day-to-day indicating something uncontrolled within the perfusion system (data not shown). It was determined that the 4-way connector was decreasing the flow rate of the solutions and creating

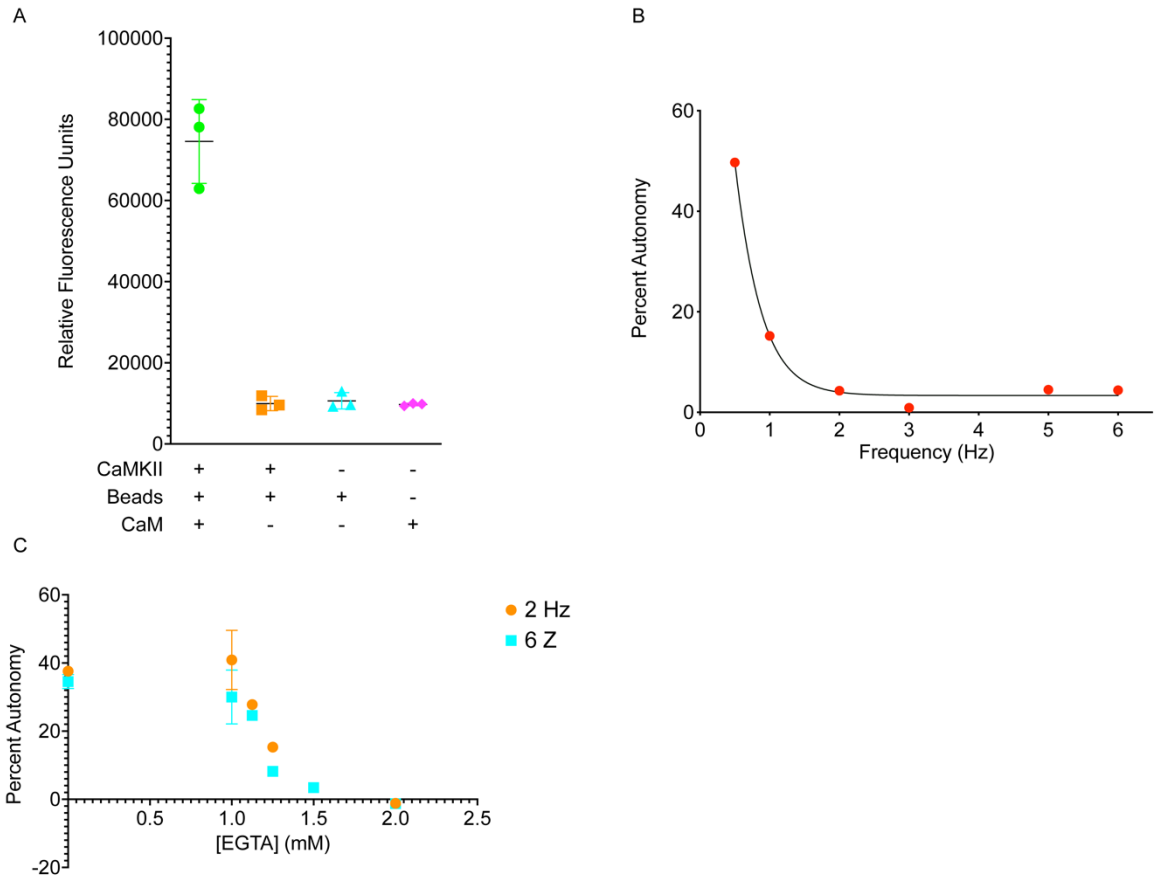

Figure 3. Optimizing conditions to obtain reproducible data from the perfusion system. A) Controls with CaMKIIα-30 bound to beads. CaMKII was not pulsed in these controls otherwise concentrations and conditions are consistent with described method. B) Frequency experiment data of CaMKIIB-30 using 8 μM CaM and 1.2 mM EGA. C) EGTA titration, 2 and 6 Hz frequency programs with 8 μM CaM and varying levels of CaM.

inconsistent consumption of reagents. I replaced this connector with a Y-connector (Fig. S6) which remedied this problem. With the perfusion system seemingly working I conducted a full set of pulse experiments with CaMKIIβ (14-16-18, 30 aa) and found high levels of autonomy at low frequencies with decreasing trend that fit to an inhibitory curve (Fig. 3B). To attempt and understand this trend, I performed an EGTA titration with CaMKIIβ-30 by conducting multiple pulse experiments at the same frequency (2 and 6 Hz) with differing concentrations of EGTA and found a sharp inhibitory response to increasing EGTA concentration (Fig. 3C). From these data, I moved forward with an EGTA concentration of 1.2 mM. However, upon repeating

frequency experiments with 1.2 mM EGTA a similar trend was observed. Thus, I moved forward with pulse duration experiments. In these experiments the frequency of the pulses remains constant, but the duration of the activation pulses changes between experiments (Fig. S7).

The pulse duration experiments produced reproduceable results. Interestingly, the variable linker increased the autophosphorylation of CaMKIIα with CaMKIIα-30 and -41 reaching higher levels of autonomy than CaMKIIα-0 (Fig. 4, S10). In addition, the variable linker increased the autophosphorylation of CaMKIIβ with CaMKIIβ-30 reaching 70% autonomous activity in comparison to 60% for CaMKIIβ-0 (Fig. 4; S10).

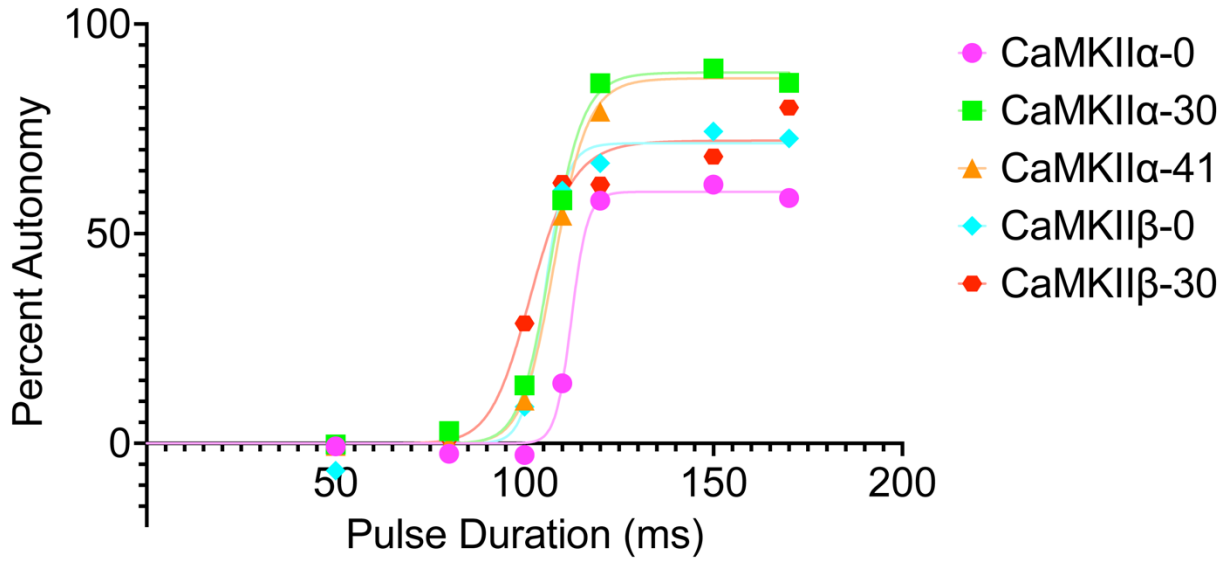

Figure 4. CaMKII decodes Ca2+ pulse duration into different levels of autonomous activity. Pulse experiments at 1 Hz ranging from 50 ms to 170 ms. Total exposure time to Ca^{2+}/CaM is consistent throughout all programs. The programs range from 120 pulses to 35 pulses. Each activating pulse is followed by a 50 ms EGTA (1.2 mM) pulse, despite the length of the activating pulses. Autonomy determined within each replicate. Single replicate data is fitted to EC_{50} equation despite being endpoint readings; fit only for ease of visualization no values from fit are used for analysis. Raw values plotted as bar graph in Figure S10.

Discussion

These data add addressing the ability of CaMKII to decode Ca^{2+} oscillations may raise more questions than they answer. First, the results raise many questions about the perfusion system. The reduction in autonomy observed when conducting a frequency titration on CaMKIIβ-30 (Fig. 3B) is completely contradicting previous results (Bayer et al., 2002; De Koninck and Schulman, 1998; Dupont et al., 2003) and intuitions. Because the total exposure time to Ca^{2+}/CaM must remain the same between pulse experiments, as the pulse duration or frequency increases, the total length of the program decreases (Fig. S7). Therefore, it seems that the EGTA pulses were not effectively chelating Ca^{2+} from the activating pulses and the decrease in autonomy could be explained by a reduction in the exposure time to Ca^{2+}/CaM i.e., the length of each program. However, when conducting a pulse experiment at 6 Hz without EGTA, 40% autonomy was measured (Fig. 3C) suggesting that this is not what is occurring. To address these confounding data, an EGTA titration was conducted at 6 Hz and 2 Hz which revealed an extremely tight gap in EGTA concentration where the autonomy was between the relative maximum and minimum. As a result 1.2 mM EGTA was implemented from the 1 mM previously used (Chao et al., 2011). However, I was still unsure about the kinetics controlling the data retrieved from the frequency experiments, so it was determined to move in another direction.

To salvage the experimental set-up, the pulse experiments were changed. Instead of increasing the frequency of pulses, the duration of activating pulses would be increased at a given frequency. Previously this provided a sigmoidal curve indicating cooperative binding of CaM and cooperative CaMKII autonomous activity (De Koninck and Schulman, 1998; Dupont et al., 2003) which is congruous with the results obtained herein. Interestingly, between CaMKIIα-30

and CaMKIIα-41 there was no significant difference between the autonomy levels (Fig. 4). Consistent with observations at saturating Ca^{2+} conditions (Sloutsky et al., 2020), we observed higher levels of autonomous activity in CaMKIIα-30 and CaMKIIα-41 than CaMKIIα-0 at similar pulse durations. This indicates that CaMKIIα-0 is less sensitive to the tested Ca^{2+} oscillations than CaMKIIα-30 and CaMKIIα-41. This result is consistent with the hypothesis that the variable linker domain tunes the activation properties of CaMKIIα (Chao et al., 2011; Sloutsky et al., 2020). However, in the context of CaMKIIβ we observed no difference in the sensitivity to pulse duration, which was unexpected but consistent with previous results (Sloutsky et al., 2020). However, there was a difference in the maximal autonomy reached at 1 Hz. CaMKIIβ-0 reached lower levels of autonomy at saturating pulse durations than CaMKIIβ-30 (Fig. 4). Although pulse duration was not explicitly tested for specific CaMKIIβ variants previously, the difference in autonomy observed at 1 Hz is consistent with previous results (Bayer et al., 2002).

These results allow for speculation about the rates of autophosphorylation between CaMKII variants. Because the total exposure time to Ca^{2+}/CaM is consistent with different pulse durations at 1 Hz, differences in the levels of autonomous activity at high pulse duration indicate a sort of saturation at certain frequencies. Thus, specific CaMKII variants can decode Ca^{2+} oscillations into specific levels of autonomy, although it would be required to replicate these initial assays and extend these experiments to more frequencies. However, it is difficult to be confident if this assay is measuring only autonomous activity because of T286 phosphorylation. Compared to previous work (Bayer et al., 2002; De Koninck and Schulman, 1998; Dupont et al., 2003) this assay yielded much higher levels of autonomous activity. Additionally, phospho-mimetic

mutation T286(D) yields only about 40% CaMKII activity in the absence of Ca^{2+}/CaM (Özden, personal communication).Therefore, it would seem the activity measured by this assay is not entirely autonomous, and CaM remains bound to CaMKII due to an increased affinity for the regulatory segment following T286 phosphorylation (Meyer et al., 1992). This result is still interesting and suggests CaMKII variants and genes differentially trap specific levels of CaM through phosphorylation of T286. In addition, when comparing these results to the V_{max} recorded by Sloutsky et al. (2020) a similar trend is observed (Fig. S8). In general, CaMKIIα variants displayed higher V_{max} than the tested CaMKIIβ variants. Additionally, the chimeric proteins displayed similar V_{max} to CaMKIIα variants. While V_{max} is very dependent upon the enzyme concentration the k_{cat} of the CaMKII kinases are unknown and may provide valuable information to understand the observed differences between CaMKIIα and CaMKIIβ activation.

The results obtain from the perfusion system are confusing and inconsistent, and there are several possibilities which may explain the results. The first issue is that the system is too large (by volume), so a single pulse does not travel all the way to the sample. Over the course of the program the pulses will reach the sample, but the amount of time between these events depends both on the frequency and the pulse duration. As a result, there is an arbitrary amount of mixing between Ca^{2+}/CaM and EGTA resulting in likely inconsistent levels of Ca^{2+}. The pulse duration experiments yielded high quality data from single replicates, but I believe this is likely due to saturation of the 50 ms EGTA (1.2 mM) pulse. The amount of Ca^{2+}/CaM released with each pulse corresponds linearly to the duration of the pulse. Thus, by increasing the Ca^{2+}/CaM without increasing EGTA, the chelating ability acts as an arbitrary threshold after which CaMKII activity will be recorded. To remedy this the volume of the system must be reduced, but the smallest

system volume is limited by fittings and necessary tube lengths. Additionally, increasing the pressure of the system above 6 PSI may fix these issues. However, increasing the pressure will also increase the reagent volume required by these experiments, which are already extremely expensive with respect to their CaM usage. Further, the increase in pressure may result in decreased recovery of CaMKII/beads which increases the noise within the kinase assay and fluorescent measurements. Therefore, this experimental design may not be the most effective way to assess the transphosphorylation rates of different CaMKII variants and their ability to decode Ca^{2+} oscillations.

Nonetheless, there are several controls which should be conducted to verify these results. Specifically, the levels of autonomy are calculated by treating a pulsed sample with Ca^{2+}/CaM and assuming this is the maximum activity of this sample. However, phosphorylation at T305/306 prevent CaM binding (Hanson and Schulman, 1992). Thus, if any phosphorylation of T305/306 occurred during a pulse experiment it would artificially increase the percent autonomy calculated by reducing the fluorescence of the maximally activated kinase reactions. It is unlikely this is what is occurring during the pulse experiments because there is no decreasing trend in fluorescent values for the maximally activated samples as pulse duration increases. However, it is a necessary control to run the same procedure with a T305/306V mutant to ensure autophosphorylation at these sites is not interfering with the calculations. T286D pulse experiments would also provide a good indication of whether the measurements are indicative of autonomy only or Ca^{2+}/CaM dependent activity. In addition, it is obvious that this data needs to be replicated an extended for more CaMKIIβ variants., especially those previously explored by Bayer et al. (2002). Lastly, although some *in vitro* analysis of Ca^{2+} transduction by CaMKII has

been conducted (Chang et al., 2017). Extending this analysis to specific splice variants, using conditional knockouts, may allow for dissection of the contributions of specific splice variants to long term potentiation in neurons.

CHAPTER III

DE NOVO CAMK2D MUTATIONS IMPACT SENSITIVITY TO CA^{2+}/CAM

Matthew J. Dunn[1], Bao Nguyen[1], Margaret M. Stratton[2]

Molecular and Cellular Biology Graduate Program[1], Department of Biochemistry and Molecular Biology[2]

Abstract

Ca^{2+}-calmodulin dependent protein kinase II (CaMKII) plays an integral role in Ca^{2+} signaling throughout the body. CaMKII is encoded by four highly conserved genes: α, β, γ, and δ which are differentially expressed in an array of tissues. As a result, dysregulation of expressed CaMKII variants can lead to a variety of human diseases. Specifically in the hippocampus, CaMKII is essential for learning and memory. Historically, only mutations within CaMKIIα and CaMKIIβ have been implicated with neurological disorders. However, with the inception of new sequencing technologies a number of mutations in all four genes have been associated with severe neurological disorders. Although expression levels of CaMKIIγ and CaMKIIδ are lower than CaMKIIα and CaMKIIβ in adult human brain it seems they are crucial for neurodevelopment. Several *de novo* mutations in CAMK2D were detected in individuals with severe disability. Most of these mutations are located within the kinase and regulatory domains. In collaboration with Geeske van Woerden we aimed to characterize the impacts of three mutations (Q274P, R275H, F294S) on the sensitivity of CaMKIIδ to Ca^{2+}/CaM. We demonstrated that all three mutations increase the sensitivity of CaMKIIδ to Ca^{2+}/CaM. Additionally, we demonstrated that Q274P and F294S demonstrate kinase activity in the absence of Ca^{2+}/CaM. The characterization of these mutations is essential for our understanding of the role CaMKII plays in human disease and neurological development.

Introduction

CaMKIIα and CaMKIIβ are essential for spatial learning and memory (Silva et al., 1992; Borgesius et al., 2011). *De novo* mutations within CaMKIIα and CaMKIIβ cause intellectual disability in humans (Küry et al., 2017). Many of these mutations are associated with aberrant protein stability, T286 phosphorylation, and migration within neurons and can act as dominant negative mutants (Küry et al., 2017; Stephenson et al., 2017). Due to its ability to form high order multimeric holoenzymes CaMKII is particularly susceptible to dominant negative effects (Bergendahl et al., 2019). Further, the exchange of subunits between active CaMKII holoenzymes allows for Ca^{2+} independent activation of subunits (Bhattacharyya et al., 2016 ; Stratton et al., 2014). However, this mechanism likely contributes further to the dominant negative effects associated with these mutants. Specifically, CaMKIIα E183V, a disease-associated mutation, is able to subunit exchange with wild-type CaMKIIα (Stephenson et al., 2017). The combination of a destabilized mutant CaMKIIα encoded by one allele with wild-type CaMKIIα encoded by another allele may result in destabilization of the entire holoenzyme leading to these dominant negative phenotypes.

On the other hand, the role of CaMKIIδ and CaMKIIγ in neuronal function and development are not well established, and until recently, mutations within these genes were not believed to affect neurodevelopment (Onori et al., 2018). Specifically, Onori et al. (2018) revealed that CaMKIIγ R292P acts as a pathogenic gain-of-function mutation causing inappropriate neuronal maturation and arborization. More recently, CaMKIIδ mutations (Q274P, R275H, and F294S) have been detected in patients with a variety of disabilities (van Woerden, personal communication). When overexpressing these mutants in induced pluripotent stem cell (iPSC) derived neurons (Küry et

al., 2017) there was no reduction in the levels of expression compared to wild-type CaMKIIδ-62 (van Woerden, personal communication). When comparing the levels of Thr286 phosphorylation from iIPSC-derived neurons, Q274P was associated with increased autophosphorylation, whereas R275H and F294S did not present drastic variations from wild-type. Q274P and R275H did not affect CaMKIIδ neuronal migration, but F294S caused a severe migration deficit. Additional interrogation of these mutants is required because R275H did not impact these assays but was detected in three unrelated patients, suggesting pathogenicity. Also, F294S revealed no drastic changes in stability or Thr286 phosphorylation but drastically impacted migration in neurons (van Woerden, personal communication). Lastly, Q274P demonstrated gain of function (van Woerden, personal communication) which has been previously associated with CaMKII pathogenicity (Onori et al., 2018).

Mutagenesis-based characterization of CaMKII activation allows for interrogation of the molecular basis of disease-causing mutations within all four CAMK2 genes. A metric which is often used to quantify CaMKII activity is EC_{50}, (Chao et al., 2011; Sloutsky et al., 2020) the concentration of Ca^{2+}/CaM required for half-maximal activation. The aim of this study to characterize the impacts of *de novo* CaMKIIδ mutations associated with severe disability on CaMKIIδ activity *in vitro*. Following completion of these assays additional experiments intend to describe the impacts of these mutations on CaMKII holoenzyme stability. Thereby, we will better understand the role of CaMKIIδ in human disease and how disease-associated mutants impact CaMKIIδ function in the brain.

Methods and Materials

Plasmid construction

Constructs built utilizing exon gene blocks (IDT) and pre-existing pSMT3 vectors containing N-terminal 6xHis followed by a SUMO tag and full-length CaMKII variants via Gibson Assembly. Mutants cloned via site-directed mutagenesis and confirmed via Sanger sequencing (GeneWiz).

Dual Expression System Cloning

Constructs built by inserting gene blocks (IDT) corresponding to Glutathione S-transferase (GST) Tag and PreScission protease site and Strep II – SUMO fusion tag with Ulp1 protease site into multiple cloning site (MCS) -1 and MCS-2, respectively, located within pETDuet-1 (gift from Mafu Lab). CaMKII genes were amplified from pre-existing pSMT3 plasmids and positioned at the C-terminal end of the protease sites via Gibson assembly. Constructs were confirmed with nanopore single-read sequencing (Plasmidsaurus).

CaMKII Expression and Purification

A previously established bacterial expression system (Choa et al., 2010) for CaMKII by coexpression with Lambda Phosphatase was utilized. We expressed CaMKII in *Escherichia coli* by coexpressing with λ phosphatase (from Kuriyan Lab) in Rosetta (DE3)pLysS competent cells (Novagen). λ phosphatase was expressed via a pCDFDuet1 vector and N-terminally clones 6xHis AviTag CaMKII was expressed in a pET287 vector. Cells were grown to an O.D. (595 nm) of 0.6 and induced with 1 mM isopropyl β-D-1-thiogalactopyranoside (IPTG; GoldBio). Cells were grown for 16 hours at 18 °C and resuspended in buffer A [25 mM tris-HCl (pH 8.5), 150 mM KCl, 50 mM imidazole, 10% glycerol; Sigma] with 25 mM magnesium chloride,

containing a cocktail of protease inhibitors and deoxyribonuclease (DNase) [0.2 mM 4 benzenesulfonyl fluoride hydrochloride (AEBSF), 5.0 μM leupeptin, pepstatin (1 μg/ml), aprotinin (1 μg/ml), trypsin inhibitor (0.1 mg/ml), 0.5 mM benzamidine, DNase (1 μg/ml)] (Sigma). Resuspended cells were flash frozen until used.

Cells were lysed via a French press and clarified cell lysate was aspirated from cell debris following centrifugation (18,000 rpm; 4 °C; 60 min). All subsequent purification steps were performed with an ÄKTA pure chromatography system (Cytiva Life Sciences) at 4 °C. Clarified cell lysate was loaded onto 2 5-mL HisTrap FF NiNTA Sepharose columns (Cytiva Life Sciences) and eluted with a combination of 50% buffer A and 50% buffer B [25 mM tris-HCl (pH 8.5), 150 mM KCl, 1 M imidazole, 10% glycerol] for a final concentration of 0.5 M imidazole. The eluate was desalted of residual imidazole with a HiPrep 26/10 Desalting column, and His SUMO tags were cleaved with Ulp1 protease overnight at 4°C in buffer C [25 mM tris-HCl (pH 8.5), 150 mM KCl, 2 mM tris(2-carboxyethyl)phosphine (TCEP) (GoldBio), 50 mM imidazole, 10% glycerol]. Cleaved tags were removed by a subtractive NiNTA step. Subsequently, and anion exchange step was performed with 2 5-mL HiTrap Q-FF (Cytiva Life Sciences) and protein was eluted with a KCl gradient. Eluted proteins were visualized via SDS-PAGE and select fractions were concentration and further purified in gel filtration buffer [25 mM tris-HCl (pH 8.0), 150 mM KCl, 1 mM TCEP, 10% glycerol] using a Superose 6 Increase 10/300 size exclusion column (Cytiva Life Sciences). Fractions were visualized by SDS-PAGE, and pure fractions were pooled, concentrated, aliquoted, flash-frozen in liquid nitrogen, and stored at -80 °C until used. Protein concentration was calculated using absorbance (280 nm).

Calmodulin Purification

Calmodulin (*Gallus gallus*) was recombinantly expressed from a pET-15b vector (a gift from A. Nairn, Yale School of Medicine) in BL21(DE3) cells (Millipore). Cells were grown to an O.D. (595 nm) of 0.6 and induced with 1 mM isopropyl β-D-1-thiogalactopyranoside (IPTG; GoldBio). Cells were grown for 16 hours at 18 °C and resuspended in cell lysis buffer [40 mM tris-HCl (pH 8.0), 100 mM KCl, 10 mM EDTA]. Resuspended cells were flash frozen until used. Cells were lysed via a French press and clarified cell lysate was aspirated from cell debris following centrifugation (18,000 rpm; 4 °C; 60 min). All subsequent purification steps were performed with an ÄKTA pure chromatography system (Cytiva Life Sciences) at 4 °C. Clarified cell lysate was loaded onto 2 5-mL HiTrap Phenyl FF (Low Sub) columns (Cytiva Life Sciences). Column flow through was collected and $CaCl_2$ was added to the flow through (final concentration 20 mM $CaCl_2$). The flow through was applied to a different pair of 5-mL HiTrap Phenyl FF (Low Sub) columns (Cytiva Life Sciences) with buffer A [50 mM tris-HCl (pH 7.5), 1mM $CaCl_2$]. The column was washed sequentially with buffer A, buffer B [50 mM tris-HCl (pH 7.5), 500 mM NaCl, 1 mM $CaCl_2$], and buffer A. Calmodulin was eluted with buffer C [50 mM tris-HCl (pH 7.5), 2 mM EDTA]. Purity was assessed via SDS-PAGE and clean eluate fractions were pooled and concentrated. To quantify calmodulin concentration, we used circular dichroism on a Jasco J-1500 spectrophotometer to make a measurement in triplicate for our purified sample scanning a wavelength spectrum between 250 and 215 nm to measure the characteristic wavelength of 222 nm as previously described (Harmat et al., 2000). We calculated the calmodulin concentration as follows:

$$[calmodulin](nM)\frac{1000 \times (CD_{sample}^{222\ nm} - CD_{blank}^{222\ nm})}{\Theta \times l \times number\ of\ amino\ acids}$$

where the circular dichroism at 222 nm (CD222nm) is expressed in mdeg, Θ is the molar ellipticity, and l is the path length in cm.

Coupled Kinase Assay

Kinase activity was monitored under previously described conditions (Chao et al., 2011; Barker et al., 1995) with a Synergy H1 microplate reader (BioTek). Each well of the plate contained master mix composed of the following (all concentrations listed as final, working concentrations): 5 mM tris (pH 7.5; Thermo Fisher Scientific), 150 mM KCl (Sigma), 10× tris/MgCl2 buffer (50 mM/10 mM, respectively) (Thermo Fisher Scientific), 0.2 mM CaCl2 (Sigma), 1 mM phosphoenolpyruvate (Alfa Aesar), nicotinamide adenine dinucleotide (0.15 mg/ml; Sigma), pyruvate kinase (10.0 U/ml; Sigma), lactate dehydrogenase (30 U/ml; Millipore Sigma), 2.0 mM adenosine triphosphate (ATP) (Sigma), and 0.3 mM syntide (LifeTein). The final pH in each well of the reaction was~7.5 to 8, and the final enzyme concentration was 13.3 nM. The reagents were added to the well in the following order: tris buffer, calmodulin (ranging from 0.4 nM to 2 μm final concentration), and mastermix. The additional of CaMKII was used to initiate the kinase reaction, after which absorbance (340 nm) was measured at 15-s intervals for 10 min. The change in absorbance over time was fitted with a straight line (y = mx + c) to obtain a slope (m) proportional to the kinetic rate of the reaction. For each time series, slopes were fitted to a sliding window of five points (1 min 15 s) and the maximum observed slope was used to represent the kinetic rate of that reaction. Kinetic rates across a series of calmodulin concentrations were fitted with the following equation:

$$Y = Y_{min} + \frac{(Y_{max} - Y_{min}) \times X^{n_H}}{X^{n_H} + EC_{50}^{n_H}}$$

to obtain EC50 (defined as the calmodulin concentration needed to reach the half-maximal reaction velocity) and cooperativity values (Hill coefficients, nH). Ninety-five percent confidence intervals for fit parameters (EC50 and nH) were determined using the following bootstrap procedure. Ten thousand replicate calmodulin concentration series were generated by randomly selecting one observed kinetic rate at each measured calmodulin concentration from the set of replicates for that variant. Each generated concentration series was fit with the equation

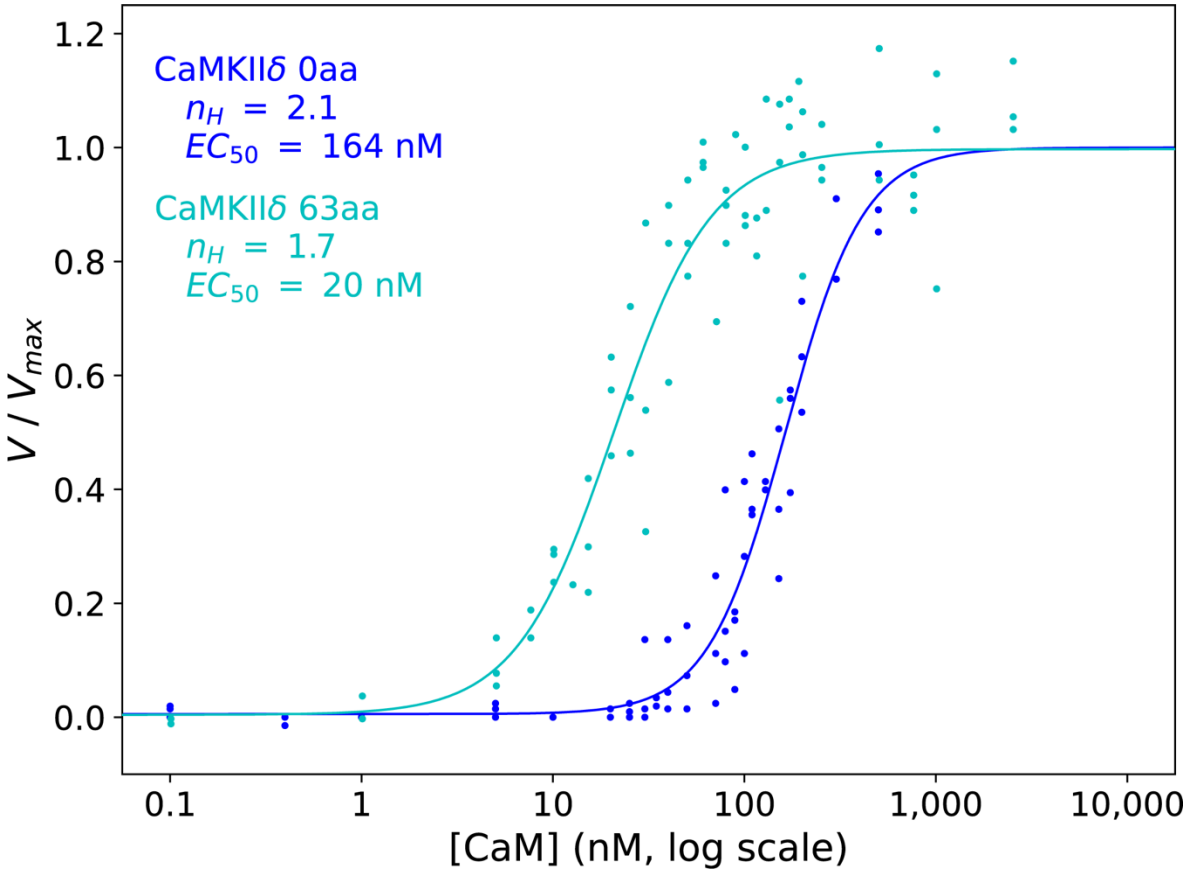

Figure 5. CaMKIIδ kinase assay results suggest variable linker tunes autoinhibited equilibrium and CaM accessibility. Kinase assay data completed and fitted as described by Sloutsky et al. Introduction of a variable linker in CaMKIIδ reveals a similar trend to CaMKIIα as previously described by Chao et al. (2011) and Sloutsky et al. (2020).

described earlier. Parameter values at the 2.5th and 97.5th quantiles of the 10,000 fits were taken as the boundaries of the 95% confidence interval.

Results

In conjunction with previous kinase assay data (Chao et al., 2011; Sloutsky et al., 2020), a CaMKIIδ variant containing a linker (6v1-14a-16-17-18, 63 aa) displayed a reduced EC_{50} when compared to a CaMKIIδ variant containing no linker (CaMKIIδ-0) (Fig 4). Sloutsky et al. (2020) reported an EC_{50} value of 167 nM for CaMKIIδ-0. In comparison, CaMKIIδ-63 displayed an EC_{50} for Ca^{2+}/CaM of 20 nM. Further, mutants of CaMKIIδ-63 – specifically, Q274P, R275H, and F294S – all displayed lower EC_{50} values 8 nM, 11 nM, and 7 nM respectively. However, these EC_{50} values do not seem to be significantly different from wild type CaMKIIδ-63. Interestingly, CaMKIIδ-63 Q274P and CaMKIIδ-63 F294S displayed Ca^{2+}/CaM independent activity. In the absence of Ca^{2+}/CaM, CaMKIIδ-63 Q274P displayed 40% activity of CaMKIIδ-63 wildtype, whereas CaMKIIδ-63F294S displayed 20% activity of CaMKIIδ-63 wildtype (Fig. 6 and 7).

To address the dominant negative impacts of CaMKII mutants a dual expression system needed to be established to allow for purification and quantification of hetero-oligomers. To develop the system, it was decided to begin with two CaMKII variants which are known to express well in our bacterial expression system CaMKIIα-0 and CaMKIIβ-0. Initially, glutathione S-tramferase (GST-tag) was fused to the N-terminus of CaMKIIβ-0 with a PreScission protease site located between them. In a similar manner, Strep-II tag was fused with

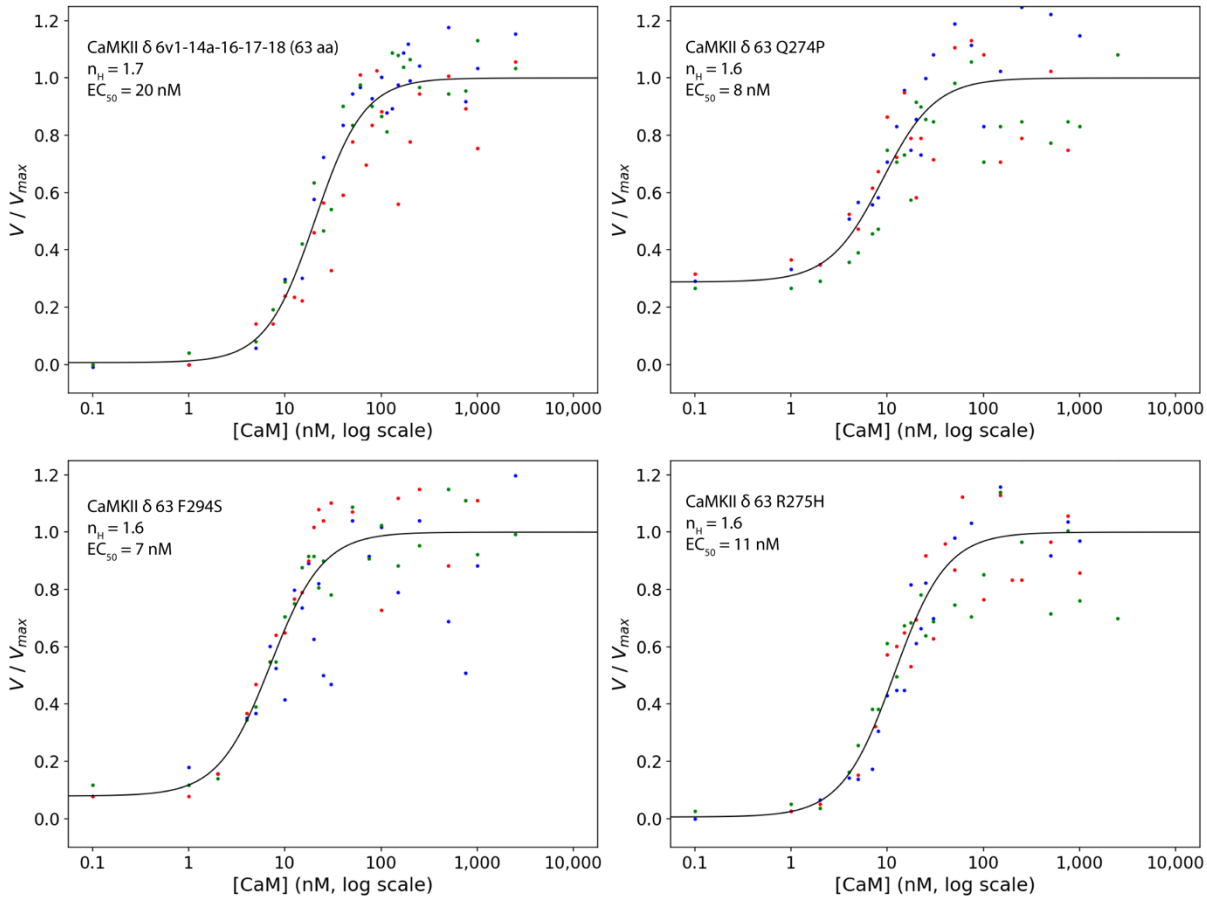

Figure 6. Mutant CaMKIIδ-63 kinase assay fits. Kinase assay data completed and fitted as described by Sloutsky et al. All mutations resulted in further decrease in EC_{50} values which are lower than any values previously determined.

the N-terminus of CaMKIIα -0 with a Tobacco Etch virus (TEV) cleavage site located between them. These two fusion proteins were cloned in pETDuet-1 and expressed as described above. Under these conditions expression CaMKIIβ-0 fused with GST is observed but there was no accumulation of CaMKIIα -0 at any time point (Fig. 9). To increase stability of CaMKIIα -0 SUMO-tag was inserted between the Strep-II tag and the N-terminus of CaMKIIα -0. The addition of SUMO did not increase the expression of CaMKIIα -0 under the same growth conditions (Fig. 9). Further development of this expression system is necessary.

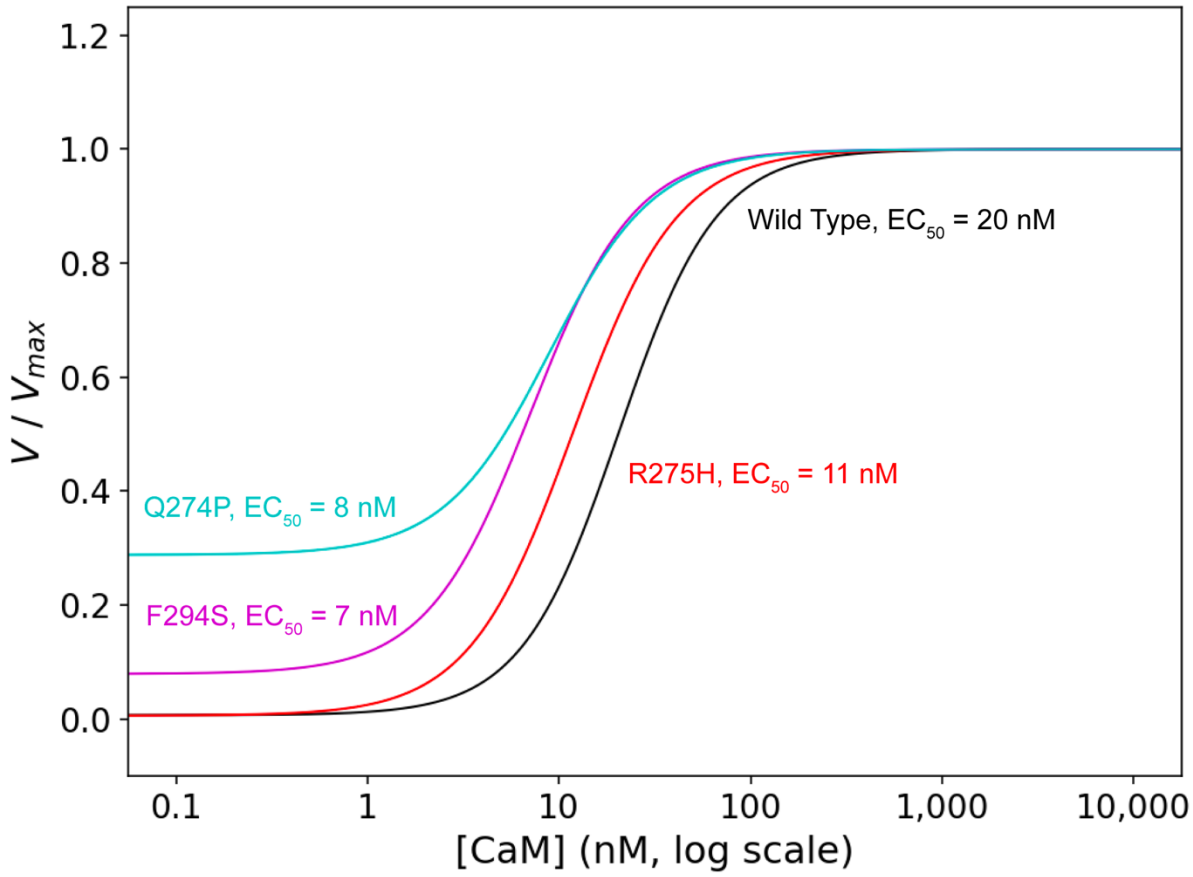

Figure 7. De novo CaMKIIδ mutations significantly impact Ca^{2+}/CaM independent activity. Data are normalized to the wild-type CaMKIIδ-63 V_{max} to reveal differences in CaMKII activity in the absence of CaM.

Discussion

The model for a tunable autoinhibited equilibrium proposed by Chao et al. (2011) was initially established in the context of CaMKIIα, but it is still applicable in this case. In fact, it may be more applicable to CaMKIIδ than to either CaMKIIβ or CaMKIIγ based on the divergence history of CaMKII paralogs and that CaMKIIβ sensitivity to Ca^{2+}/CaM is not influenced by the presence of the variable linker (Sloutsky et al., 2020). Both Chao et al. (2011) and Sloutsky et al. (2020) demonstrate an increase in the sensitivity of CaMKIIα to Ca^{2+}/CaM when any linker is present. While the presence of a linker – not the length – determined CaMKIIα sensitivity to

Ca^{2+}/CaM (Sloutsky et al., 2020) , the composition of the linker has been shown to vastly impact CaMKIIα sensitivity to Ca^{2+}/CaM (Nguyen, personal communication). Thus, more data would be needed to determine if the linker length and composition within CaMKIIδ variants further impacts sensitivity to Ca^{2+}/CaM (Fig. 5). Additionally, there is a slight reduction of the hill coefficient

(n_H) value

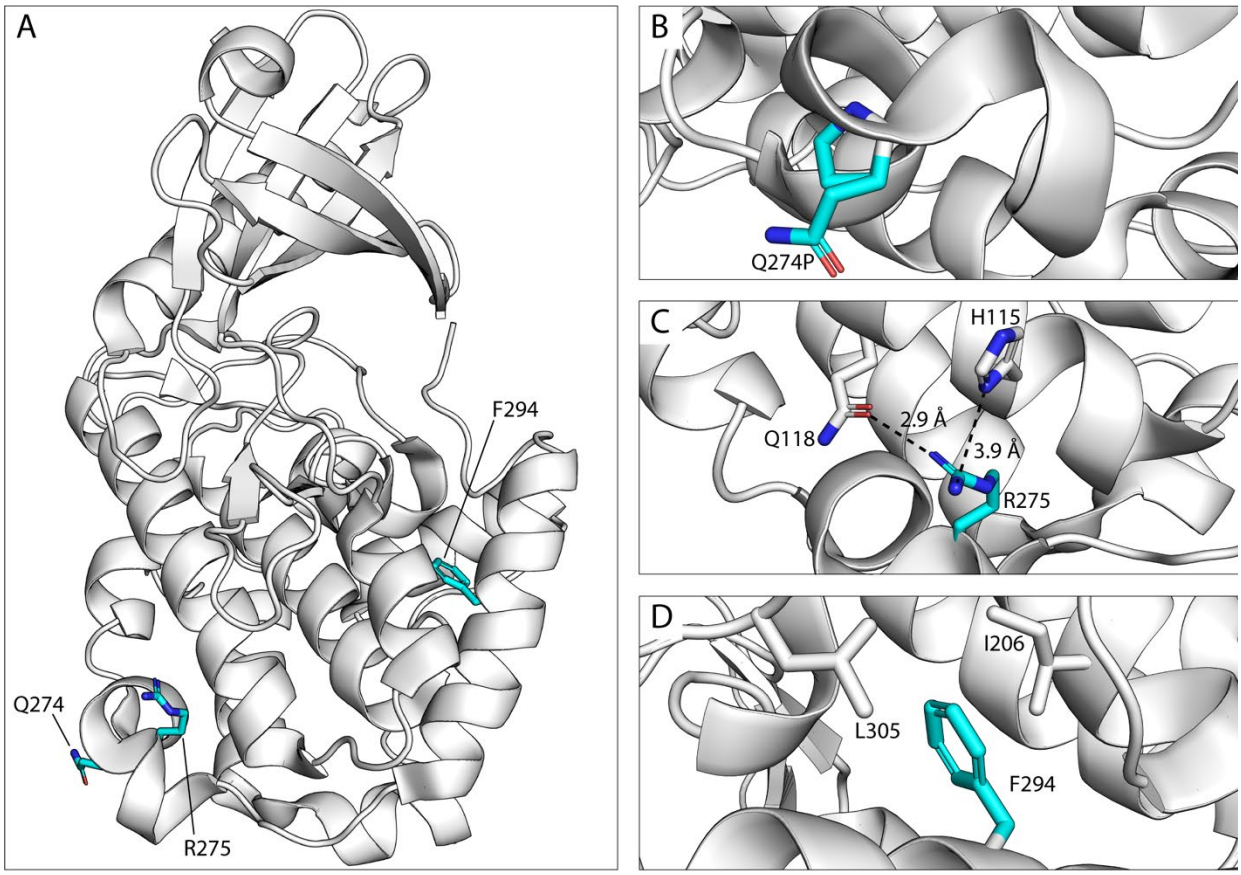

Figure 8. Analysis of structural impacts caused by de novo mutations on CaMKIIδ kinase and regulatory segment. The figures above were constructed from a crystal structure of inhibited CaMKIIδ and regulatory segment (PDB: 2VN9). **(A)** The positions of the mutations and their corresponding wild-type residues are colored in cyan. The remainder of the kinase is colored white. **(B)** Q274 is located within a unique alpha helical turn and solvent exposed. This image shows an overlay of Q274 and P274 indicating the potential positioning of a proline directly in the helical turn. **(C)** R275 is located within the same turn and is proximal enough to Q118 for hydrogen bonding (2.9 Å) and H115 (3.9 Å) for like-charged pair interaction (Heyda et al., 2010) between the two nitrogen atoms. **(D)** F294 is located within the regulatory segment and faces into a hydrophobic patch consisting of I206 and L305.

reported by Sloutsky et al. (2020) for CaMKIIδ-0 (n_H = 2.3) compared to these variants (n_H = 1.6-1.7). This is likely related to the quality of the fits, but these values still indicate cooperative binding of CaM and CaMKII activation (Chao et al., 2010).

The increase in Ca^{2+}/CaM independent activity of these mutants (Q274P, R275H, and F294S) provides some evidence about the structural importance of these residues (PDB: 2VN9 (Rellos et al., 2010)). These residues are conserved across all four CaMKII genes excluding position 274 which is Histidine in CaMKIIα but remains solvent exposed (PDB: 3SOA (Chao et al., 2010)). Q274 and R275 are located within a small alpha helix amino-terminal to the autoinhibitory domain (Fig. 8A). This alpha helical turn seems to be crucial for the correct positioning of the autoinhibitory domain. Proline is an uncommon residue in helices and often results in their early termination (Chou and Fasman, 1974). Therefore, substitution of glutamine to proline at position 274 (Fig. 8B) would likely break this alpha helix and disrupt proper orientation of the autoinhibitory domain resulting in a CaMKII protein that is more easily activated. The results from the kinase assays are consistent with this hypothesis and reveal that this mutation allows for activity of CaMKII in the absence of Ca^{2+}/CaM (Fig. S9).

The adjacent residue, R275, is also required for positioning of the autoinhibitory segment and conserved across all four genes. Previous mutagenesis of R274 in CaMKIIα to glutamate resulted in a 5% increase in Ca^{2+}-independent activity (Yang and Schulman, 1999) suggesting that integrity of this smaller alpha helix affects CaMKII activation. In CaMKIIδ, H115 and Q118 are proximal to R275 and could form interactions which stabilize the position of the alpha helix

(Fig. 8C). In particular, the interaction formed between R275 and H115 may be a like-charged pair interaction (Heyda et al., 2010) caused by π-π interactions. Specifically, the introduction of H-H π-stacking caused by 275H would be associated with a higher entropic cost because it requires more rigidity and precise orientation of the histidine side chains (Heyda et al., 2010). It is likely that R275H would not completely disrupt this helical turn but may affect proper orientation of the autoinhibitory segment. The slight reduction in EC_{50} for R275H when compared to CaMKII CaMKIIδ-62 is consistent with this hypothesis, however this mutation does not induce Ca^{2+}/CaM independent activity as the others do.

Lastly, F294 is located within the main alpha helix of the autoinhibitory segment, which is highly conserved across all four human CaMKII genes (Rellos et al., 2010). Upon further inspection of the crystal structure of CaMKIIδ kinase and regulatory domain, the sidechain of F294 is facing inwards toward a hydrophobic patch in the kinase domain (Fig 7D). The distance between these residues (L305 4.3 Å; I206 4.5 Å) is within the range for Van der Waals interactions. Previous mutagenesis of key positions within the regulatory segment indicated that conservation of the residues which interface with the kinase domain is integral for CaMKII activity (Yang and Schulman, 1999). Specifically, F294E resulted in no increase in Ca^{2+}-independent activity but did increase affinity for CaM (Yang and Schulman, 1999). On the contrary, I observed a slight increase in Ca^{2+}/CaM independent activity. Therefore, mutating F294 likely disrupts interactions with the kinase domain and may lead to some Ca^{2+}/CaM-independent activity and increased sensitivity to Ca^{2+}/CaM. This hypothesis may explain the reduction in EC_{50} (Fig. 6 and 7) and the Ca^{2+}/CaM independent activity which was observed for F294S (Fig. S9)

These mutations appear to be more active than wild-type CaMKIIδ and may act as gain-of-function mutants *in vivo*. *De novo* mutations that were previously detected in CaMKIIα and β both increase and decrease T286 phosphorylation which negatively impacts migration of CaMKII in neurons (Küry et al., 2017). More recently, a gain of function mutation, R292P, which is associated with intellectual disability was detected in CaMKIIγ (Onori et al., 2018). These mutations (Q274P, R275H, and F294S), therefore, are consistent with previous observations that many CaMKII mutants responsible for human disease impact CaMKII activation properties. These mutants also seem to impact the stability of CaMKIIδ due to reduced expression of all three mutants in E. coli. Obviously more precise biophysical characterization of stability is necessary, but these mutants likely also impact holoenzyme stability and protein turnover thereby impacting CaMKII signaling *in vivo*.

Further study of *de novo* CaMKII mutations and their impacts on CaMKII activity *in vitro* and *in vivo* is necessary. In particular, the formation of hetero-oligomers with CaMKII occurs in vivo (Brocke et al., 1999) and is important for targeting of CaMKII. Thus, the expression of mutant and wildtype CaMKII within the same cell likely occurs and impacts kinase activity and holoenzyme stability and turnover. To test these properties the development of a dual expression system would be beneficial and allow for purification of recombinant heterooligomers even if we cannot control the exact stoichiometries.

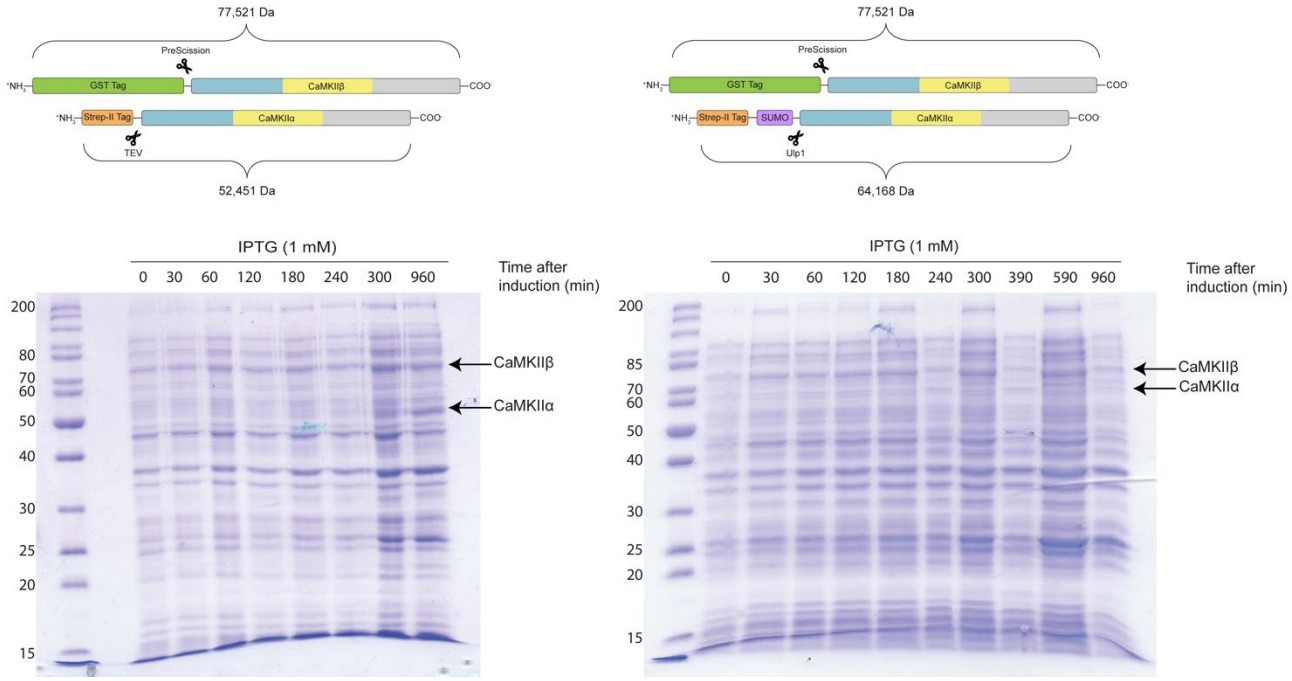

Figure 9. pETDuet-1 dual expression system design and expression tests. Linear depictions of the two constructs to be coexpressed are shown above the corresponding gels. The gel images are representative of samples taken following induction with 1 mM IPTG. Number to the left of the gel images correspond with the molecular weight (kDA) of the markers. On the right side of each gel are arrows which highlight bands corresponding to the predicted molecular weight of the two CaMKII constructs. The lanes for each gel are as follows (time in minutes following induction): LEFT): 0, 30, 60, 120, 180, 240, 300, 960; RIGHT): 0, 30, 60, 120, 180, 240, 300, 390, 585, 960.

The design of the dual expression system had two parts in mind, to be able to discern the CaMKII variants from one another by size and to be able to specifically select for a species containing both variants – should one exist. With these goals in mind, I began with pETDuet-1 which allows for very simple cloning strategies to be implemented. Two CaMKII genes were inserted into the multiple cloning sites (MCS). Next, I chose two tags which differed in weight but were highly specific, glutathione s-transferase (GST) tag and Strep tag. This would allow for the two CaMKII constructs do be easily identified and subsequent pull downs from these tags would allow for purification of only heterooligomers. For the initial test of this system, I chose two variants which express well: CaMKIIα-0 and CaMKIIβ-0. GST was fused with the N-terminus of CaMKIIβ-0 and Strep-II with the N-terminus of CaMKIIα-0. In addition, protease

sites – PreScission and TEV, respectively – were included between the tags and the N-terminus (Fig. 9). The plasmid was expressed as normally and time points were taken throughout the growth, however only expression of CaMKIIβ-0 was observed (Fig. 9). This could possibly be due to the increased stability and solubility associated with GST fusion proteins (Smith, 2000). To increase the expression of CaMKIIα-0, a SUMO tag was inserted between the Strep tag and the N-terminus. However, this did not increase the expression of CaMKIIα-0. Further troubleshooting of this system is necessary.

CHAPTER IV

FREQUENCY EXPERIMENT COMPLETE PROTOCOL

Matthew J. Dunn[1], Margaret M. Stratton[2]

Molecular and Cellular Biology Graduate Program[1], Department of Biochemistry and Molecular Biology[2]

Protocol

Buffers

Frequency Buffer

- 150 mM KCl
- 50 mM tris-HCl, pH 7.5

EGTA Buffer

- 1.2 mM EGTA
- 25 mM tris-HCl, pH 8.0

10X tris-HCl, Mg2+ Buffer

- 500 mM tris-HCl, pH 7.5
- 100 mM MgCl2

Bead Preparation and Incubation

1. Determine necessary volume of beads for the number of pulse experiments you will be conducted.
    a. 10 μL of beads per each pulse experiment (i.e., 4 pulses = 40 μL of beads)
2. Remove beads from fridge and place on ice. Prior to removing beads homogenize them by swirling container in your hand until no beads remain sedimented on the bottom of the container.

3. Transfer the necessary volume of beads to a clean tube.
4. Add volume of Frequency Buffer for 10 X total volume (i.e., 400 μL for 40 μL of beads)
5. Concentrate the beads with a magnet and remove buffer 'supernatant'. Discard Buffer.
6. Repeat Steps 4 and 5 two more times for a total of 3 washes.
7. After washes, resuspend beads in frequency buffer, protein, and 100 mM TCEP.
    a. [Final TCEP] = 1 mM
    b. Protein mass should be calculated to saturate the beads. (10mg/mL; >2,500 pmol/mg beads)
    c. Add Frequency Buffer up to 10x volume of beads.
8. Incubate protein and beads for 1.5 h at 4 °C, rotating at 20 rpm.

Activation and Master Mix Preparation

1. ADP Hunter Reagents mut equilibrate at room temperature for at least 1 hour before use, so take them out and thaw them immediately after beginning protein/bead incubation. If necessary, combine multiple aliquots into one tube and mix prior to use.
2. Additionally, remove 100 mM ATP aliquots and CaM stock from -20 and -80, respectively, to allow time to thaw on ice.
3. At 6 PSI and using the y-connector you need ~9 mL of Activation Buffer for the pulse experiments (60, 100 ms pulses). Additionally, you will need several mL to fill the system.
    a. Therefore, volume of activation buffer = 2 + 9*(# of pulse experiments)
4. The Activation Buffer components are as follows (Add them in this order and mix after each reagent):
    a. Frequency Buffer

b. 20 mM $CaCl_2$ – [Final] = 500 μM

c. CaM (concentration prep dependent) – [Final] = 8 μM

d. 100 mM ATP – [Final] = 250 μM

e. 500 mM $MgCl_2$ – [Final] = 10 mM

Calculations for necessary volumes can be found in benchling (Matt -> Notebook -> Frequency Experiments).

5. Store Buffer on ice until use.
6. 4 μL of Master Mix is added to each kinase reaction. Normally 6 kinase reactions are run per pulse experiment + and additional 3 of reagents only to begin each experiment)
    a. Volume = 4*6*(# of pulse experiments) +3
    b. You want to make more than the exact volume you need.
7. Syntide is the determining reagent for how much you make. The reactions use very little syntide (< 1mg) so the increments on the scale are 0.1 mg.
8. Determine the amount of syntide needed for your experiment and weigh it using the scale in the Heuck lab. Ensure the mass is accurate.
9. Resuspend the syntide in the necessary volume of 100 mM tris-HCl, pH 8.0
10. Combine the following reagents in a clean tube for master mix:
    a. 1.5 mM Syntide – [Final in Kinase Reaction] = 300 μM
    b. 2 mM ATP – [Final in Kinase Reactions] = 100 μM
        i. Dilute 100 mM ATP to 2 mM ATP with 100 mM tris-HCl, pH 8.0
    c. 10X tris-HCl, Mg^{2+} Buffer – [Final in Kinase Reactions] = 75/15 mM
11. Dilute remaining CaM to 100 μM.

a. Only need 2 μL of 100 μM CaM for each pulse experiment so a minimal volume is necessary.
b. Dilute CaM with 25 mM tris-HCl pH 8.0, 500 μM $CaCl_2$

Pulse Experiment

1. Following incubation of the protein/beads, concentrate beads with magnet and remove supernatant. Keep Supernatant.
    a. A good control to test binding is to run a +CaM kinase assay with this and compare the activity to your beads, the dilutions will be slightly off but still a good thing to check if you get weird results.
    b. This will allow for you to approximate the amount of protein that bound.
2. Resuspend beads in 10X bead volume of Frequency buffer and mix.
3. Concentrate the beads with a magnet and remove buffer 'supernatant'. Discard Buffer.
4. Repeat Steps 2 and 3 two more times for a total of 3 washes.
5. Resuspend beads in 10.05x bead volume of frequency buffer. For each frequency experiment you will use 100 μL of beads, so this will give you enough for each one.
6. Fill each syringe with buffer:
    a. Just make sure you have enough of EGTA and Frequency
    b. Each pulse experiment uses about 9 mL of Activation Buffer so ensure you have enough.
7. Connect the air supply to each syringe and ensure that channel 2 (the empty one is close). Then turn on the air supply. Adjust the pressure if necessary to 6 PSI using the dial on top of the perfusion system.

8. Flow 2 mL of each buffer through the system using the manual mode on the controller.
9. Secure the injection loop to the magnet.
    a. First turn the T-connector such that it closes the injection loop from the rest of the system.
    b. Use three pieces of tape to attach the tubing to the rim of the magnet. At this point about half of the tubing will be secured to the magnet. You can double check that you have secured the correct amount of tubing by inserting the needle into the tubing and seeing that it reaches just the end of the taped area.
10. Next, fill the injection loop with frequency buffer.
    a. Use needle and 1 mL syringe to fill loop with frequency buffer.
    b. IT IS CRUCIAL TO REMOVE ALL AIR FROM THE INJECTION LOOP. Any air which is left in the loop will significantly decrease the recovery of your beads.
    c. The volume of frequency buffer used doesn't matter just make sure the loop is filled without any air
11. Apply your beads to the tubing.
    a. Remove 100 μL of beads from your stock and transfer to a clean microcentrifuge tube.
    b. Use same needle and 1 mL syringe to remove beads from tube.
    c. When injecting onto the tubing ensure no air in the syringe.
    d. If you place the syringe directly next to the magnet the beads will remain in the needle, so to avoid this stop the end of the needle just below the area of tape tubing and deposit your beads slowly.

e. If done correctly you should see your beads accumulate right where the taped portion of the tubing ends.

f. Add 400 µL of frequency buffer to the tube which contained your 100 µL of beads and use this volume to wash the syringe. Mix up and down. Apply total volume to the injection loop as described previously.

g. Following application of your sample, very carefully tape the remaining tubing to the rim of the magnet.

12. Open the T-connector such that the injection loop is connected to the perfusion system.
13. Double check all connectors are open, buffer volumes, and pressure.
14. Run appropriate pulse experiment.
15. Disconnect Activation and EGTA Y connector and switch to Frequency Buffer.
16. Place the end of the tube in a microcentrifuge tube and remove the tape holding the tubing to the magnet. Flick the now free tubing with the end in the microcentrifuge tube. Then run program 10 (300 ms pulse of Frequency Buffer) to elute any beads which are somewhat stuck.
17. Use the magnet to concentrate your beads as previously described. Remove ALL supernatant and resuspend beads in 35 µL of cold frequency buffer. (You use 5 µL per kinase reaction and will run 6 reactions per pulse experiment so this allows you to have enough plus some extra in case)
18. Turn off the air and depressurize the system.

ADP Hunter Plus Kinase Reactions

1. For each pulse experiment run:
    a. 2 + CaM reactions

b. 4 – CaM reactions

c. Run at least 2 baseline reactions (reagents/Buffer only) for the whole day

2. To each reaction add:

    a. 4 µL master mix

    b. 1 µL 100 µM CaM or 25 mM Tris pH 8.0

    c. Add 5 µL of pulsed beads

3. It is crucial to begin a timer when adding kinase to the first reaction. Then space your additional reactions by 20 s. You should finish adding kinase to 4 reactions in 1 min (0s, 20 s, 40s, 60s)

4. Following addition or kinase to all reactions you will quench the kinase reaction with 2 µL of 50 mM EDTA, 15 mM EGTA after 5minutes. So, at 5 minutes add the quench buffer to the first reaction and space by 20 s again to keep the reaction time consistent.

5. After you have quenched all of the reactions, add the ADP Hunter reagents, Solution A and Solution B immediately after one another

    a. Add 5 µL Solution A and 10 µL of Solution B to the same well.

    b. Try to keep the addition of solution A + B spaced the same for all reactions

6. Following the addition of the ADP Hunter reagents to all reactions start a 15-minute timer and cover the plate with tin foil

7. Also move your ADP Hunter reagents back to dark storage.

8. Take a reading using the plate reader

    a. The protocol is a fluorescent intensity, endpoint reading

    b. The excitation is 530 and emission is 590

    c. Keep all other parameters as the preset

9. Export your data to whatever place you want to process
10. To calculate percent autonomy, you should average the values of each condition.
11. Then subtract the average baseline fluorescent value from the average frequency fluorescent and the maximum fluorescent.
12. Finally divide your adjusted frequency fluorescent average by the adjusted maximum fluorescent average for your percent autonomy.
13. To conduct replicates, you should repeat the pulse experiment itself for technical replicates.

SUPPLEMENTARY FIGURES

Figure S1. Normalized CaMKIIα N-terminal AviTag construct kinase assay fits. Data was normalized as in Sloutsky et al. (2020).

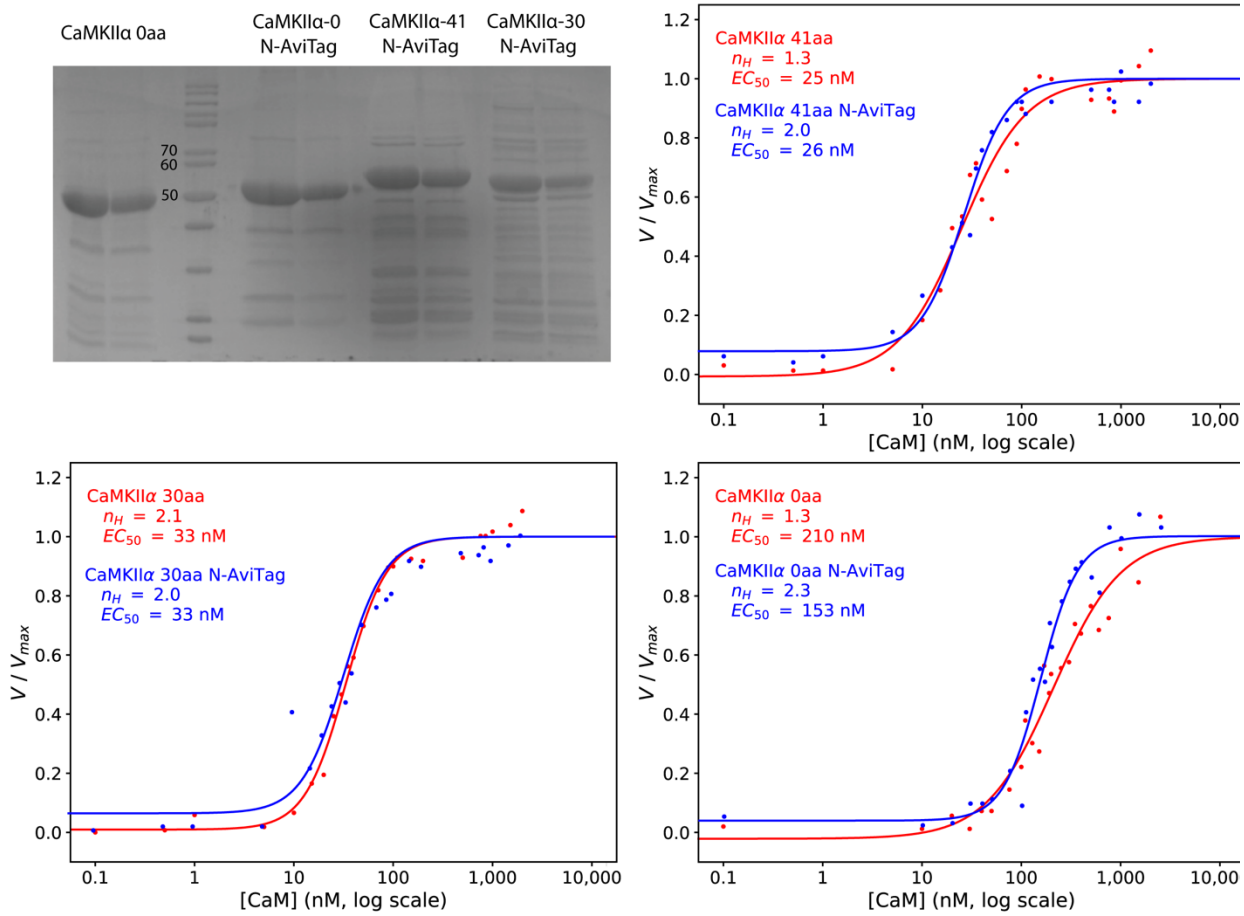

Figure S2. Normalized CaMKIIβ N-terminal AviTag construct kinase assay fits. Data was normalized as in Sloutsky et al. (2020).

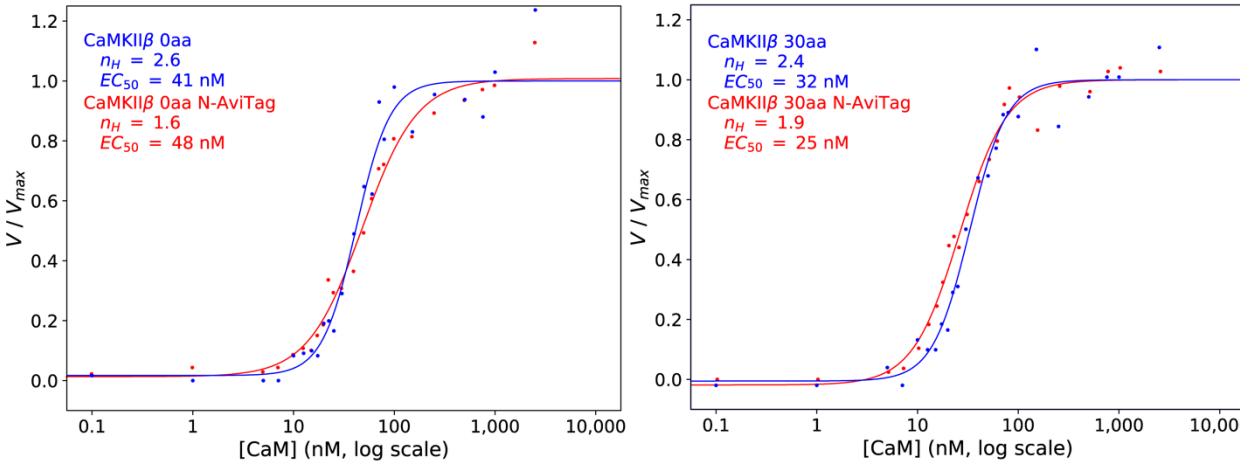

Figure S3. Parameters from EC50 fits of N-terminal AviTag constructs.

Variant	Linker Length	Spliced-In Linker Exons	EC_{50}	n_H	V_{max}
α1	41	14, 15, 18	25.0	1.35	1.522
α2	30	14, 18	33.4	2.09	1.816
α0	0	none	210.6	1.28	1.655
α1 N-AviTag	41	14, 15, 18	26.3	2.00	0.325
α2 N-AviTag	30	14, 18	30.4	1.32	0.991
α0 N-AviTag	0	none	153.9	2.31	0.907
β7	30	14a, 8	32.9	2.36	1.011
β8	0	none	41.8	2.58	0.803
β7 N-AviTag	30	14a, 8	25.6	1.86	1.090
β8 N-AviTag	0	none	48.8	1.60	0.934

Figure S4. ADP Hunter standard curve.

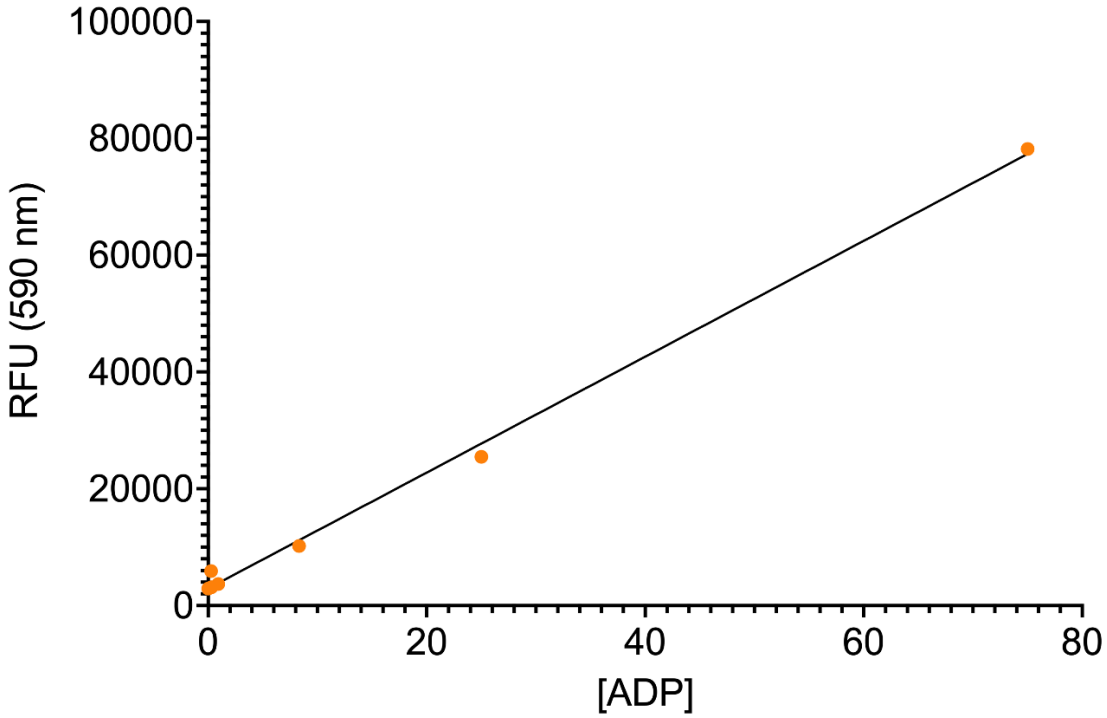

Figure S5. ADP Hunter CaMKII titration. CaMKIIα-30 was used in this titration, and it was not bound to beads, thus protein concentration is known and calculable by A280.

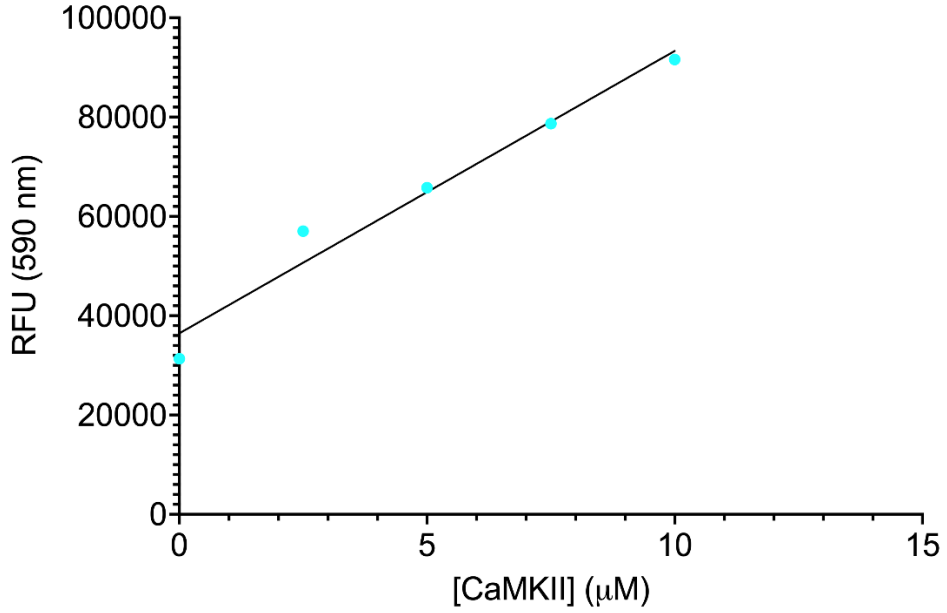

Figure S6. Technical images of perfusion system and bead injection. A) Depiction of how Y-connector and proximity to tubing for injection. Half of tubing taped to magnet prior to injection. Ensure the connector is closed to the system when injecting sample, as shown in images. B) Position of needle when injecting the sample. It is crucial not to position the needle directly next the needle or the beads will remain in the needle. Also ensure tubing has not air when injection sample.

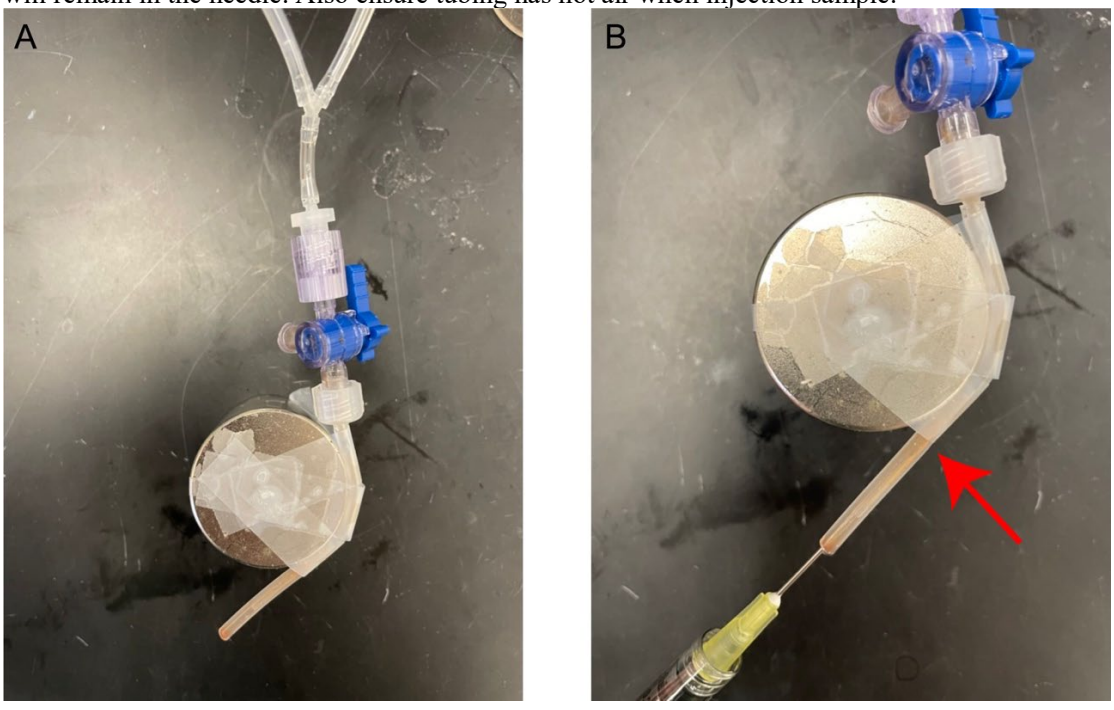

Figure S7. Visualization and comparison of frequency programs compared to pulse duration programs.

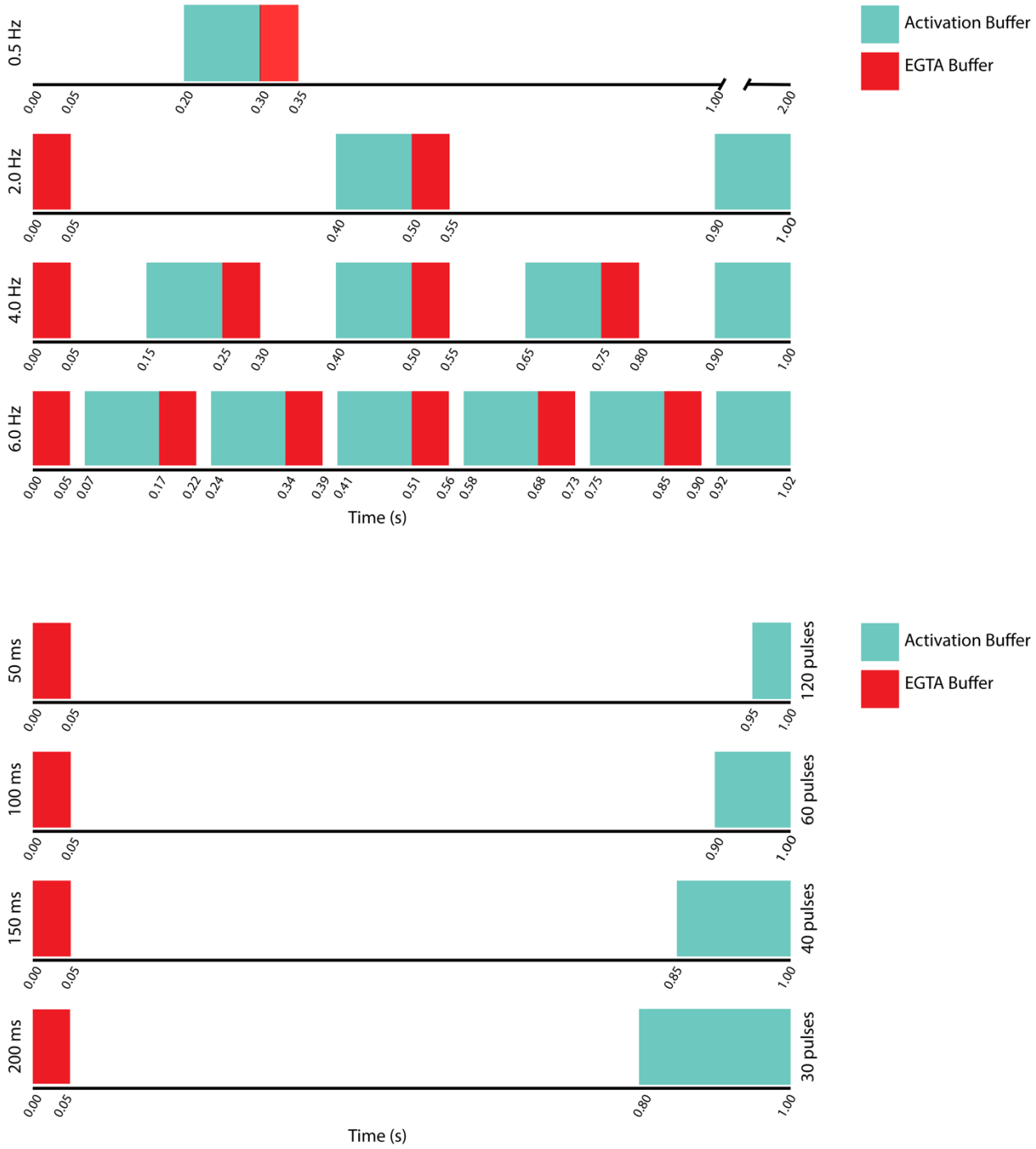

Figure S8. Fit parameters from EC50 fits determined by Sloutsky et al. (2020).

Variant	Linker Length	Spliced-In Linker Exons	EC_{50}	n_H	V_{max}
α1	41	14, 15, 18	23.2	1.45	1.373
α2	30	14, 18	22.2	1.44	1.641
α0	0	none	181.4	1.46	1.225
α kinase/ β hub	0	none	22.1	1.90	0.851
β kinase/ α hub	0	none	97.8	2.30	0.998
β1	217	13, 14b, 16, 17, 18, 19v1,2,3	17.1	2.23	1.150
β2	93	13, 14b, 16, 17, 18	19.6	1.34	0.833
β3	69	14a, 16, 17, 18	9.7	1.57	0.820
β4	68	14b, 16, 17, 18			
β5	54	14a, 16, 18	12.6	1.66	0.746
β7	93	14a, 8	19.1	0.91	
β8	0	none	18.0	1.97	0.703

Figure S9. Raw slopes of de novo CaMKIIδ mutations in the absence of CaM.

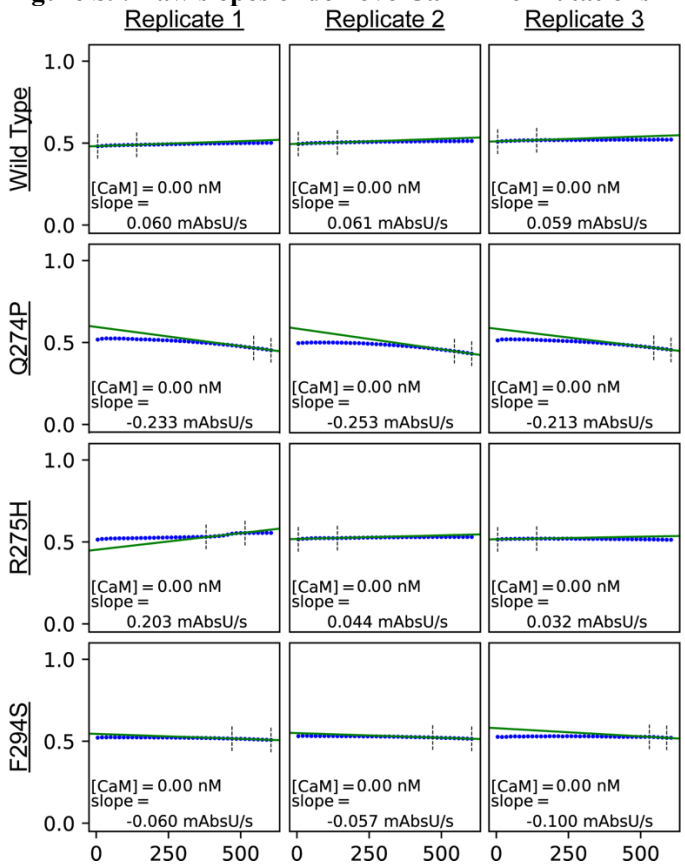

Figure S10. Raw fluorescent values of pulse duration experiments. Y axis label is relative fluorescence units. Bar graphs indicate mean and standard deviation is shown by error bars.

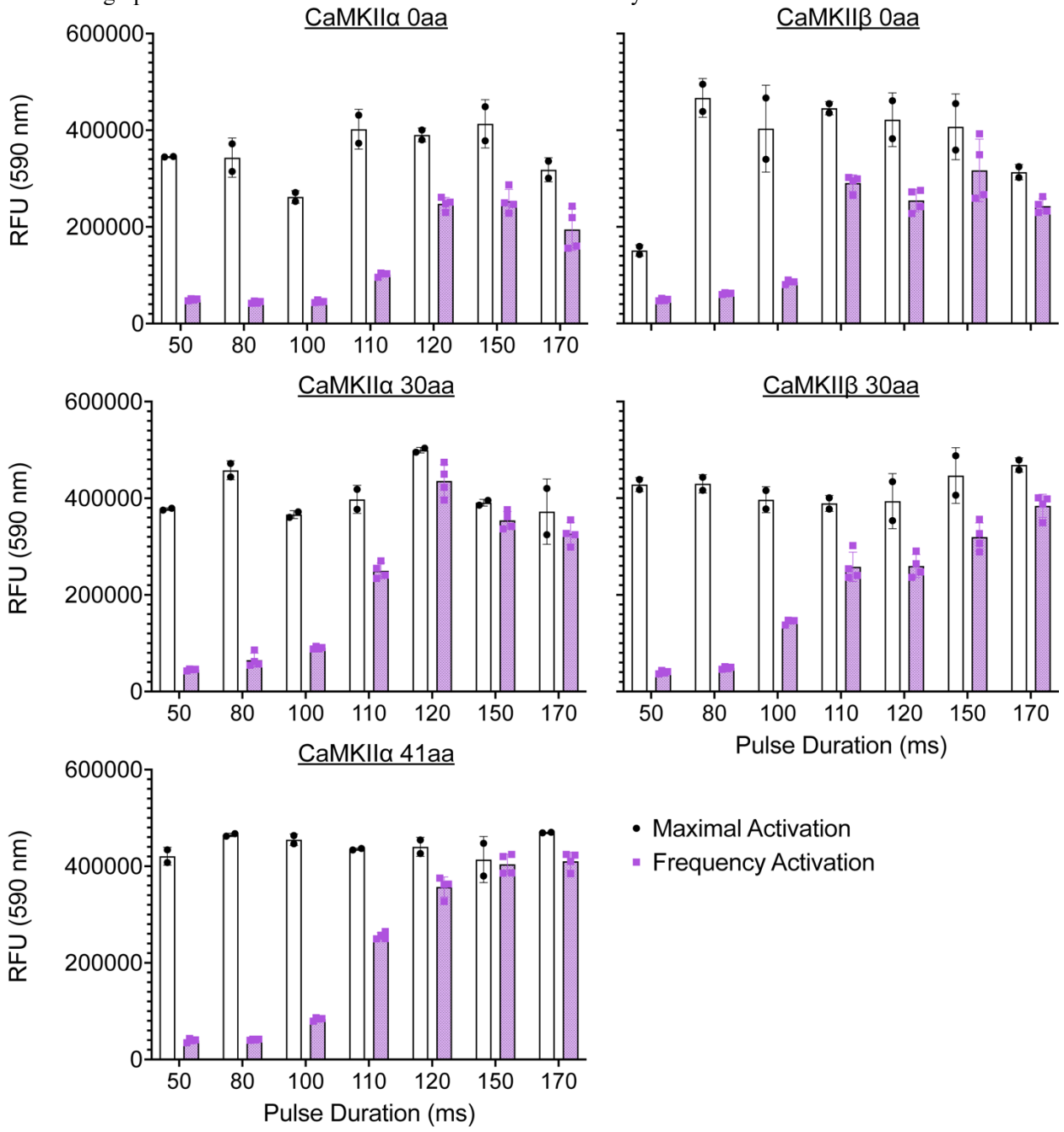

REFERENCES

Barkus, C., Sanderson, D.J., Rawlins, J.N.P., Walton, M.E., Harrison, P.J., and Bannerman, D.M. (2014). What causes aberrant salience in schizophrenia? A role for impaired short-term habituation and the GRIA1 (GluA1) AMPA receptor subunit. Molecular Psychiatry *19*, 1060–1070. https://doi.org/10.1038/mp.2014.91.

Bashir, Z.I., Alford, S., Davies, S.N., Randall, A.D., and Collingridge, G.L. (1991). Long-term potentiation of NMDA receptor-mediated synaptic transmission in the hippocampus. Nature *349*, 156–158. https://doi.org/10.1038/349156a0.

Bayer, K.U., Koninck, P.D., and Schulman, H. (2002). Alternative splicing modulates the frequency-dependent response of CaMKII to Ca2+ oscillations. The EMBO Journal *21*, 3590–3597. https://doi.org/10.1093/emboj/cdf360.

Bennett, M.K., Erondu, N.E., and Kennedy, M.B. (1983). Purification and characterization of a calmodulin-dependent protein kinase that is highly concentrated in brain. Journal of Biological Chemistry *258*, 12735–12744. https://doi.org/10.1016/S0021-9258(17)44239-6.

Bergendahl, L.T., Gerasimavicius, L., Miles, J., Macdonald, L., Wells, J.N., Welburn, J.P.I., and Marsh, J.A. (2019). The role of protein complexes in human genetic disease. Protein Science *28*, 1400–1411. https://doi.org/10.1002/pro.3667.

Bhattacharyya, M., Stratton, M.M., Going, C.C., McSpadden, E.D., Huang, Y., Susa, A.C., Elleman, A., Cao, Y.M., Pappireddi, N., Burkhardt, P., et al. Molecular mechanism of activation-triggered subunit exchange in Ca2+/calmodulin-dependent protein kinase II. ELife *5*. https://doi.org/10.7554/eLife.13405.

Bliss, T.V.P., and Lømo, T. (1973). Long-lasting potentiation of synaptic transmission in the dentate area of the anaesthetized rabbit following stimulation of the perforant path. J Physiol *232*, 331–356. .

Bliss, T.V.P., Collingridge, G.L., and Morris, R.G.M. (2014). Synaptic plasticity in health and disease: introduction and overview. Philosophical Transactions of the Royal Society B: Biological Sciences *369*, 20130129. https://doi.org/10.1098/rstb.2013.0129.

Borgesius, N.Z., Woerden, G.M. van, Buitendijk, G.H.S., Keijzer, N., Jaarsma, D., Hoogenraad, C.C., and Elgersma, Y. (2011). βCaMKII Plays a Nonenzymatic Role in Hippocampal Synaptic Plasticity and Learning by Targeting αCaMKII to Synapses. J. Neurosci. *31*, 10141–10148. https://doi.org/10.1523/JNEUROSCI.5105-10.2011.

Brown, G.P., Blitzer, R.D., Connor, J.H., Wong, T., Shenolikar, S., Iyengar, R., and Landau, E.M. (2000). Long-Term Potentiation Induced by θ Frequency Stimulation Is Regulated by a Protein Phosphatase-1-Operated Gate. J. Neurosci. *20*, 7880–7887. https://doi.org/10.1523/JNEUROSCI.20-21-07880.2000.

Catterall, W.A. (2011). Voltage-Gated Calcium Channels. Cold Spring Harbor Perspectives in Biology *3*, a003947–a003947. https://doi.org/10.1101/cshperspect.a003947.

Chang, J.-Y., Parra-Bueno, P., Laviv, T., Szatmari, E.M., Lee, S.-J.R., and Yasuda, R. (2017). CaMKII Autophosphorylation Is Necessary for Optimal Integration of Ca2+ Signals during LTP Induction, but Not Maintenance. Neuron *94*, 800-808.e4. https://doi.org/10.1016/j.neuron.2017.04.041.

Chao, L.H., Pellicena, P., Deindl, S., Barclay, L.A., Schulman, H., and Kuriyan, J. (2010). Intersubunit capture of regulatory segments is a component of cooperative CaMKII activation. Nature Structural & Molecular Biology *17*, 264–272. https://doi.org/10.1038/nsmb.1751.

Chao, L.H., Stratton, M.M., Lee, I.-H., Rosenberg, O.S., Levitz, J., Mandell, D.J., Kortemme, T., Groves, J.T., Schulman, H., and Kuriyan, J. (2011). A Mechanism for Tunable Autoinhibition in the Structure of a Human Ca2+/Calmodulin- Dependent Kinase II Holoenzyme. Cell *146*, 732–745. https://doi.org/10.1016/j.cell.2011.07.038.

Chia, P.H., Zhong, F.L., Niwa, S., Bonnard, C., Utami, K.H., Zeng, R., Lee, H., Eskin, A., Nelson, S.F., Xie, W.H., et al. (2018). A homozygous loss-of-function CAMK2A mutation causes growth delay, frequent seizures and severe intellectual disability. ELife *7*, e32451. https://doi.org/10.7554/eLife.32451.

Chou, P.Y., and Fasman, G.D. (1974). Conformational parameters for amino acids in helical, β-sheet, and random coil regions calculated from proteins. Biochemistry *13*, 211–222. https://doi.org/10.1021/bi00699a001.

Collingridge, G.L., Kehl, S.J., and McLennan, H. (1983). Excitatory amino acids in synaptic transmission in the Schaffer collateral-commissural pathway of the rat hippocampus. J Physiol *334*, 33–46. .

Crick, F. (1984). Neurobiology: Memory and molecular turnover. Nature *312*, 101–101. https://doi.org/10.1038/312101a0.

De Koninck, P., and Schulman, H. (1998). Sensitivity of CaM Kinase II to the Frequency of Ca2+ Oscillations. Science *279*, 227–230. https://doi.org/10.1126/science.279.5348.227.

Dupont, G., Houart, G., and De Koninck, P. (2003). Sensitivity of CaM kinase II to the frequency of Ca2+ oscillations: a simple model. Cell Calcium *34*, 485–497. https://doi.org/10.1016/S0143-4160(03)00152-0.

Erondu, N., and Kennedy, M. (1985). Regional distribution of type II Ca2+/calmodulin-dependent protein kinase in rat brain. J Neurosci *5*, 3270–3277. https://doi.org/10.1523/JNEUROSCI.05-12-03270.1985.

Giese, K.P., Fedorov, N.B., Filipkowski, R.K., and Silva, A.J. (1998). Autophosphorylation at Thr286 of the α Calcium-Calmodulin Kinase II in LTP and Learning. Science *279*, 870–873. https://doi.org/10.1126/science.279.5352.870.

Gleichmann, M., and Mattson, M.P. (2011). Neuronal Calcium Homeostasis and Dysregulation. Antioxid Redox Signal *14*, 1261–1273. https://doi.org/10.1089/ars.2010.3386.

Hanson, P.I., and Schulman, H. (1992). Inhibitory autophosphorylation of multifunctional Ca2+/calmodulin-dependent protein kinase analyzed by site-directed mutagenesis. Journal of Biological Chemistry *267*, 17216–17224. https://doi.org/10.1016/S0021-9258(18)41915-1.

Harmat, V., Böcskei, Z., Náray-Szabó, G., Bata, I., Csutor, A.S., Hermecz, I., Arányi, P., Szabó, B., Liliom, K., Vértessy, B.G., et al. (2000). A new potent calmodulin antagonist with arylalkylamine structure: crystallographic, spectroscopic and functional studies11Edited by R. Huber. Journal of Molecular Biology *297*, 747–755. https://doi.org/10.1006/jmbi.2000.3607.

Herring, B.E., and Nicoll, R.A. (2016). Long-Term Potentiation: From CaMKII to AMPA Receptor Trafficking. Annu. Rev. Physiol. *78*, 351–365. https://doi.org/10.1146/annurev-physiol-021014-071753.

Heyda, J., Mason, P.E., and Jungwirth, P. (2010). Attractive Interactions between Side Chains of Histidine-Histidine and Histidine-Arginine-Based Cationic Dipeptides in Water. J. Phys. Chem. B *114*, 8744–8749. https://doi.org/10.1021/jp101031v.

Kennedy, M., McGuinness, T., and Greengard, P. (1983a). A calcium/calmodulin-dependent protein kinase from mammalian brain that phosphorylates Synapsin I: partial purification and characterization. J Neurosci *3*, 818–831. https://doi.org/10.1523/JNEUROSCI.03-04-00818.1983.

Kennedy, M.B., Bennett, M.K., and Erondu, N.E. (1983b). Biochemical and immunochemical evidence that the “major postsynaptic density protein” is a subunit of a calmodulin-dependent protein kinase. Proc Natl Acad Sci U S A *80*, 7357–7361. .

Kerchner, G.A., and Nicoll, R.A. (2008). Silent synapses and the emergence of a postsynaptic mechanism for LTP. Nat Rev Neurosci *9*, 813–825. https://doi.org/10.1038/nrn2501.

Küry, S., van Woerden, G.M., Besnard, T., Proietti Onori, M., Latypova, X., Towne, M.C., Cho, M.T., Prescott, T.E., Ploeg, M.A., Sanders, S., et al. (2017). De Novo Mutations in Protein Kinase Genes CAMK2A and CAMK2B Cause Intellectual Disability. The American Journal of Human Genetics *101*, 768–788. https://doi.org/10.1016/j.ajhg.2017.10.003.

Lau, C.G., and Zukin, R.S. (2007). NMDA receptor trafficking in synaptic plasticity and neuropsychiatric disorders. Nature Reviews Neuroscience *8*, 413–426. https://doi.org/10.1038/nrn2153.

Lin, Y.-C., and Redmond, L. (2009). Neuronal CaMKII acts as a structural kinase. Commun Integr Biol *2*, 40–41. .

Lisman, J.E. (1985). A mechanism for memory storage insensitive to molecular turnover: a bistable autophosphorylating kinase. Proc Natl Acad Sci U S A *82*, 3055–3057. .

Lisman, J., Schulman, H., and Cline, H. (2002). The molecular basis of CaMKII function in synaptic and behavioural memory. Nature Reviews Neuroscience *3*, 175–190. https://doi.org/10.1038/nrn753.

Lisman, J., Yasuda, R., and Raghavachari, S. (2012). Mechanisms of CaMKII action in long-term potentiation. Nat Rev Neurosci *13*, 169–182. https://doi.org/10.1038/nrn3192.

Meyer, T., Hanson, P.I., Stryer, L., and Schulman, H. (1992). Calmodulin Trapping by Calcium-Calmodulin-Dependent Protein Kinase. Science *256*, 1199–1202. https://doi.org/10.1126/science.256.5060.1199.

Okamoto, K.-I., Narayanan, R., Lee, S.H., Murata, K., and Hayashi, Y. (2007). The role of CaMKII as an F-actin-bundling protein crucial for maintenance of dendritic spine structure. Proceedings of the National Academy of Sciences *104*, 6418–6423. https://doi.org/10.1073/pnas.0701656104.

Onori, M.P., Koopal, B., Everman, D.B., Worthington, J.D., Jones, J.R., Ploeg, M.A., Mientjes, E., Bon, B.W. van, Kleefstra, T., Schulman, H., et al. (2018). The intellectual disability-associated CAMK2G p.Arg292Pro mutation acts as a pathogenic gain-of-function. Human Mutation *39*, 2008–2024. https://doi.org/10.1002/humu.23647.

Patterson, M.A., Szatmari, E.M., and Yasuda, R. (2010). AMPA receptors are exocytosed in stimulated spines and adjacent dendrites in a Ras-ERK–dependent manner during long-term potentiation. Proceedings of the National Academy of Sciences *107*, 15951–15956. https://doi.org/10.1073/pnas.0913875107.

Patton, B.L., Miller, S.G., and Kennedy, M.B. (1990). Activation of type II calcium/calmodulin-dependent protein kinase by Ca2+/calmodulin is inhibited by autophosphorylation of threonine within the calmodulin-binding domain. J. Biol. Chem. *265*, 11204–11212. .

Rellos, P., Pike, A.C.W., Niesen, F.H., Salah, E., Lee, W.H., von Delft, F., and Knapp, S. (2010). Structure of the CaMKIIδ/Calmodulin Complex Reveals the Molecular Mechanism of CaMKII Kinase Activation. PLoS Biol *8*. https://doi.org/10.1371/journal.pbio.1000426.

Robison, A.J. (2014). Emerging role of CaMKII in neuropsychiatric disease. Trends in Neurosciences *37*, 653–662. https://doi.org/10.1016/j.tins.2014.07.001.

Shen, K., Teruel, M.N., Subramanian, K., and Meyer, T. CaMKIIɴ Functions As an F-Actin Targeting Module that Localizes CaMKII␣/ɴ Heterooligomers to Dendritic Spines. 14. .

Shi, S.-H., Hayashi, Y., Petralia, R.S., Zaman, S.H., Wenthold, R.J., Svoboda, K., and Malinow, R. (1999). Rapid Spine Delivery and Redistribution of AMPA Receptors After Synaptic NMDA Receptor Activation. Science *284*, 1811–1816. https://doi.org/10.1126/science.284.5421.1811.

Silva, A.J., Paylor, R., Wehner, J.M., and Tonegawa, S. (1992). Impaired spatial learning in alpha-calcium-calmodulin kinase II mutant mice. Science *257*, 206–211. https://doi.org/10.1126/science.1321493.

Sloutsky, R., and Stratton, M.M. (2020). Functional implications of CaMKII alternative splicing. Eur J Neurosci ejn.14761. https://doi.org/10.1111/ejn.14761.

Sloutsky, R., Dziedzic, N., Dunn, M.J., Bates, R.M., Torres-Ocampo, A.P., Boopathy, S., Page, B., Weeks, J.G., Chao, L.H., and Stratton, M.M. (2020). Heterogeneity in human hippocampal CaMKII transcripts reveals allosteric hub-dependent regulation. Sci. Signal. *13*. https://doi.org/10.1126/scisignal.aaz0240.

Smith, D.B. (2000). Generating fusions to glutathione S-transferase for protein studies. Methods Enzymol *326*, 254–270. https://doi.org/10.1016/s0076-6879(00)26059-x.

Stephenson, J.R., Wang, X., Perfitt, T.L., Parrish, W.P., Shonesy, B.C., Marks, C.R., Mortlock, D.P., Nakagawa, T., Sutcliffe, J.S., and Colbran, R.J. (2017). A Novel Human CAMK2A Mutation Disrupts Dendritic Morphology and Synaptic Transmission, and Causes ASD-Related Behaviors. J. Neurosci. *37*, 2216–2233. https://doi.org/10.1523/JNEUROSCI.2068-16.2017.

Stratton, M., Lee, I.-H., Bhattacharyya, M., Christensen, S.M., Chao, L.H., Schulman, H., Groves, J.T., and Kuriyan, J. (2014). Activation-triggered subunit exchange between CaMKII holoenzymes facilitates the spread of kinase activity. ELife *3*. https://doi.org/10.7554/eLife.01610.

Tao, W., Lee, J., Chen, X., Díaz-Alonso, J., Zhou, J., Pleasure, S., and Nicoll, R.A. (2021). Synaptic memory requires CaMKII. ELife *10*, e60360. https://doi.org/10.7554/eLife.60360.

Tombes, R.M., Faison, M.O., and Turbeville, J.M. (2003). Organization and evolution of multifunctional Ca2+/CaM-dependent protein kinase genes. Gene *322*, 17–31. https://doi.org/10.1016/j.gene.2003.08.023.

Wollmuth, L.P., and Sakmann, B. (1998). Different Mechanisms of Ca2+ Transport in NMDA and Ca2+-permeable AMPA Glutamate Receptor Channels. J Gen Physiol *112*, 623–636. .

Yang, E., and Schulman, H. (1999). Structural Examination of Autoregulation of Multifunctional Calcium/Calmodulin-dependent Protein Kinase II *. Journal of Biological Chemistry *274*, 26199–26208. https://doi.org/10.1074/jbc.274.37.26199.

Zhang, J., and Abdullah, J.M. (2013). The role of GluA1 in central nervous system disorders. Rev Neurosci *24*, 499–505. https://doi.org/10.1515/revneuro-2013-0021.

Zhang, M., Tanaka, T., and Ikura, M. (1995). Calcium-induced conformational transition revealed by the solution structure of apo calmodulin. Nature Structural Biology *2*, 758–767. https://doi.org/10.1038/nsb0995-758.